A.I.F.A. - ITALIAN ASSOCIATION FOR FATIGUE IN AERONAUTICS

DEPARTMENT OF CIVIL AND INDUSTRIAL ENGINEERING - UNIVERSITY OF PISA

Review of aeronautical fatigue investigations carried out in Italy during the period April 2021 - March 2023

by

D. Fanteria

Department of Civil and Industrial Engineering

University of Pisa – Italy

daniele.fanteria@unipi.it

This document summarizes the principal research activities carried out in Italy about aeronautical fatigue in the period April 2021 – March 2023. The main topics covered are operational load analysis, fatigue and fracture mechanics of metals, fatigue and damage tolerance of composites, Structural Health Monitoring, NDI methods.

38th ICAF Conference, Delft, 26-29 June 2023

CONTENTS

1 INTRODUCTION 1

2 MEASUREMENT AND ANALYSIS OF OPERATIONAL LOADS 1

2.1 AM-X life monitoring (Leonardo Aircraft Division) 1

2.2 Life monitoring of the TORNADO fleet (Leonardo Aircraft Division) 2

2.3 EF Typhoon life monitoring (Leonardo Aircraft Division) 2

2.4 C-27J In-Service Life Monitoring Program (Leonardo Aircraft Division) 3

2.5 M-346 In-Service Monitoring (Leonardo Aircraft Division) 4

2.6 Rotorcraft Usage Monitoring through Machine Learning (Leonardo Helicopter Division) 5

2.7 Export Eurofighter aircraft – New setting of BSD recording start 8

3 METALS 10

3.1 Fatigue behaviour of notched and un-notched materials 10
3.1.1 Unique Materials for Advanced Aerospace Applications – UMA3 (University of Bologna) 10
3.1.2 REACH regulation implementation (Leonardo Aircraft Division) 11
3.1.3 Testing of Additively manufactured Aluminium Alloy (Leonardo Aircraft Division) 12
3.1.4 Testing of laser cut parts (Leonardo Aircraft Division) 12
3.1.5 One-up drilling process (Leonardo Aircraft Division) 13

3.2 Crack propagation and fracture mechanics 15
3.2.1 Fracture tests of friction stir welded plates machined from forged AA 2219-T851 shells (Univ. Pisa) 15

3.3 Corrosion and fatigue 17
3.3.1 Corrosion Effects Assessment on Fatigue Behaviour of Al 7475-T7351 (Leonardo Helicopter Division) 17

3.4 Structural Health Monitoring 21
3.4.1 Structural Health Monitoring – Acoustic Emissions (Univ. Bologna) 21

4 COMPOSITES AND FIBER METAL LAMINATES 22

4.1 Investigation on Disbond Arrest Features in adhesive joints (Univ. Bologna) 22

4.2 Structural Health Monitoring by means of Optical Fibres (Uni. Bologna) 24

4.3 Delamination onset resistance of composite material systems (Univ. Pisa) 26

4.4 Meso-scale models for the interaction of damage modes in composites laminates (Milan Polytech.) 27

4.5 Testing of an out of autoclave–liquid resin infused carbon-epoxy curved stiffened panel (Univ. Pisa) 30

5 NDI METHODS 33

5.1 Probability of Detection for Visual Inspection (Leonardo Helicopter Division) 33

6 AIRCRAFT FATIGUE SUBSTANTIATION 36

6.1 Fatigue related activities on AW189 (Leonardo Helicopter Division) 36

6.2 EUROFIGHTER Production Major Airframe Fatigue Test (Leonardo Aircraft Division) 36

6.3 M346 & M345 Trainers Certification status (Leonardo Aircraft Division) 37

6.4 FALCO XPLORER – Full Scale Fatigue Test (Leonardo Aircraft Division) 38

7 REFERENCES 39

1 INTRODUCTION

This paper summarises aeronautical fatigue investigations carried out in Italy during the period April 2021 to March 2023. The different contributions have been arranged according to the topics, which are operational load analysis, fatigue and fracture mechanics of metallic materials, fatigue and damage tolerance behaviour of composites, structural health monitoring and NDI methods.

The review is based on the activities carried out within the various organisations belonging to A.I.F.A., the Italian Association for Fatigue in Aeronautics. The author gratefully acknowledges the fundamental contribution, which has made this review possible, given by several A.I.F.A. members, who are the representatives of Universities and Industries in A.I.F.A.

2 MEASUREMENT AND ANALYSIS OF OPERATIONAL LOADS

2.1 AM-X life monitoring (Leonardo Aircraft Division)

As it is customary for every Italian National Review, updated information on the rate of fatigue life consumption of the AM-X fleet is given. Aircraft fatigue monitoring is based on mechanical g-meter readings and on information about configurations and mission profiles. Up to now, close to 223 thousand flight hours have been monitored since the aircraft entered service, even though the number of still active airplanes has drastically reduced (currently only 6 aircrafts are in service), and the aircraft is going to be retired from service at the end of year 2023. As shown in Figure 2.1, the rate of growth of monitored and flown hours is the same (both strike and trainer airplanes are equally monitored).

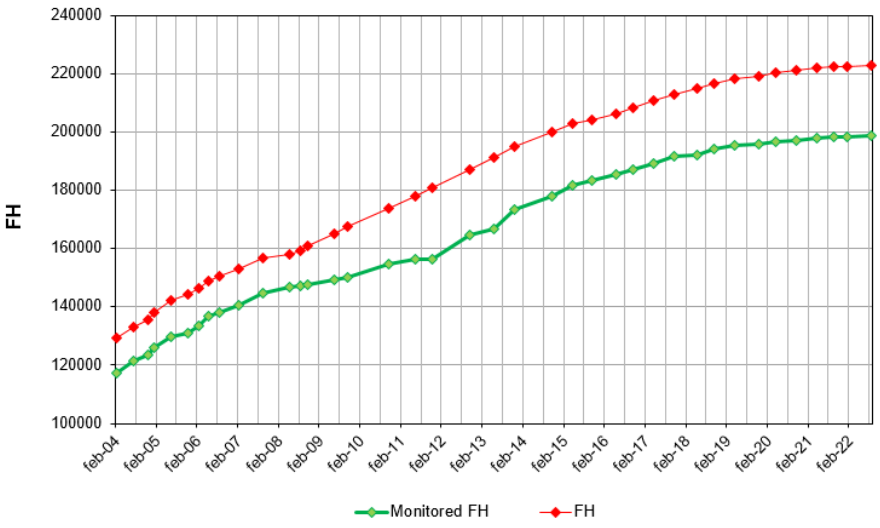

Figure 2.1 AM-X fleet monitored rates (FH): FH rate vs monitored FH rate are similar.

The parameter used for assessing the usage intensity any aircraft is the Load Severity Index (L.S.I.), defined, by Leonardo Aircraft Division, as the ratio between the damage cumulated in a flight hour and the damage caused by an average hour of the design spectrum.

The L.S.I. trend as a function of time (Figure 2.2) shows a small difference between the Strike version – with a L.S.I. index lower than 1 – and the Trainer one – which has, on the contrary, a

L.S.I. index higher than 1; the L.S.I. averaged across the whole fleet has been stably below 1 for the last 10 years.

The last period of observation confirmed the slight tendency towards lower severity utilisation rates with an average value stably at about 0.96 for the whole fleet (also due to the stably decreasing number of active aircrafts), which anyhow means that the fatigue life consumption is substantially in line with design assumptions.

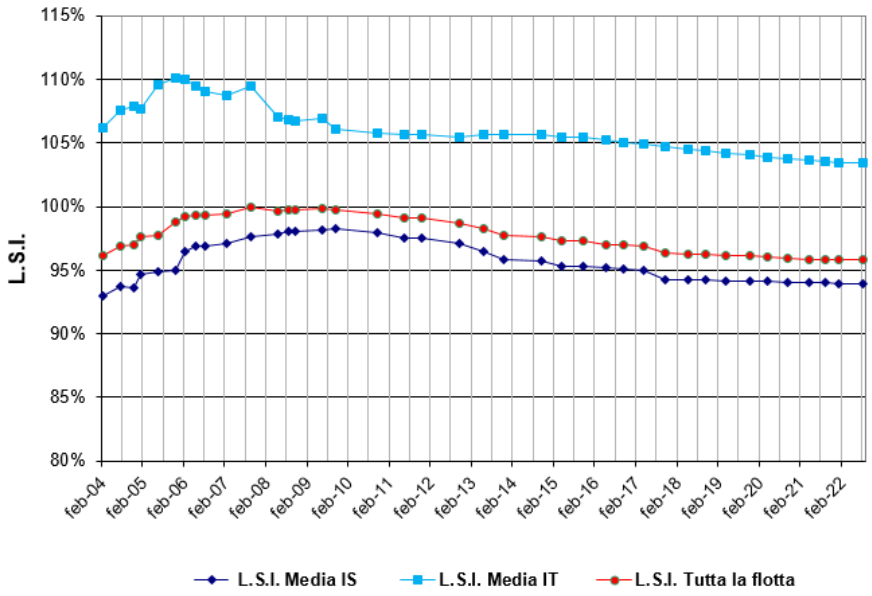

Figure 2.2 AM-X: time history of the average Load Severity Index.

2.2 Life monitoring of the TORNADO fleet (Leonardo Aircraft Division)

The Tornado programme is a consortium, led by Panavia Aircraft GmbH, with Leonardo acting as a partner company with BAE Systems and Airbus Defence and Space. The Italian Air Force acquired 99 aircrafts, that were delivered between May 1982 and July 1989, of which only 37 are still in service.

From the beginning of Tornado activity to end of 2016 Leonardo analysed about 300000 flight hours; from 2016 onward, a Maintenance Recorder System (Ma.Re.S), entered into service and, currently, Leonardo is contracted only for problems concerning Ma.Re.S malfunctioning or updating of the database due to the life extension of specific airplane components.

Up to now, the only malfunctioning was the – hardware related – non-correct reading of some parameters used by the life consumption algorithms.

The aircraft service life has been extended from 4000 to 6000 Flight Hours and the individual tracking has been maintained to assure a correct fleet management, and that any possible anomalous fatigue consumption can be promptly identified.

Currently Leonardo Aircraft Division actively participates to the life extension of German Tornado fleet up to 8000 flight hours.

2.3 EF Typhoon life monitoring (Leonardo Aircraft Division)

The whole Italian Air Force fleet of EF Typhoons is composed by 95 airplanes, 81 Single Seater (SS) and 14 Twin Seater (TS), in service since year 2003. The fleet has accumulated about 130000 Flight Hours FH, corresponding to about 82300 flights. The SS fleet leader is beyond 2560 FH while its TS counterpart has accumulated about 1600 FH.

Individual Aircraft in-service monitoring is performed by means of a Structural Health Monitoring (SHM) system that monitors ten significant locations on the structure to derive the in-service spectrum in terms of aircraft load factor (Nz) and to evaluate the Usage Factor at the monitored locations on the structure. The Usage Factor is defined as the ratio between mean hourly consumption and the design one: (Usage factor) = (in-service usage rate) / (design usage rate).

The Nz Spectrum is qualitatively reported in Figure 2.3: both SS and TS fleets are flying within the design envelope.

Figure 2.3 Non-dimensional Nz spectrum of the IAF Typhoon fleet.

Figure 2.4 shows that the Usage Factor rate is below the design value for all the 10 locations.

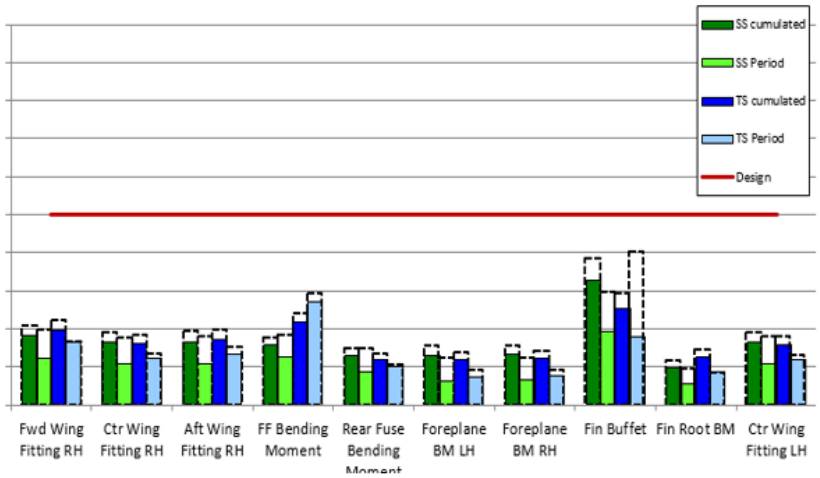

Figure 2.4 Usage Factor for the 10 monitored locations.

The trend is a decrease in all locations, as can be seen from the fact that the column relevant to the value in the period (typically 6 months) is often shorter than the one relevant to the cumulated average, i.e. the average value from the beginning of the monitoring. The lead location is number 8, for both SS and TS.

2.4 C-27J In-Service Life Monitoring Program (Leonardo Aircraft Division)

This section gives an update on the C-27J monitoring activity for the Italian Air Force that has already been presented in previous National Reviews. The active fleet is composed of 12 aircraft

and at the latest available update (April 2022) a total of about 34200 flights had been monitored for 47160 flight hours, overall.

The monitoring is performed through a specifically developed Individual Aircraft Tracking Program (I.A.T.P.) software, that runs on ground; the software monitors the fatigue life of each aircraft based on the actual mission profiles and load spectra determined by means of the direct recording of in-flight parameters.

The I.A.T.P. software monitors the main representative locations of structural items through the calculation of the Load Severity Index (LSI), which is the ratio between the In-Service Life Damage and the Design Life Damage. The Design Life Damage is the fatigue damage calculated under theoretical mission profiles and mixing, which were applied during the full-scale fatigue testing. In conclusion, the LSI measures the different severity among in-service and design usage.

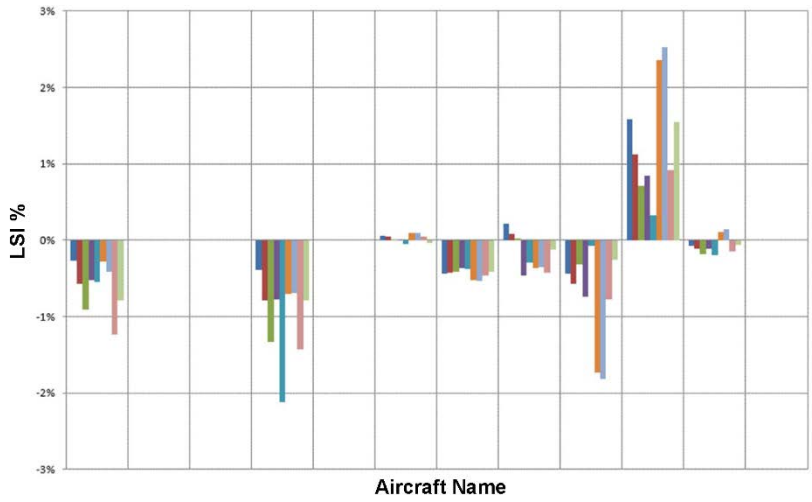

Figure 2.5 LSI percentage variation at monitored locations over the last period.

Figure 2.5 shows, for a few individual airplanes, the trend of LSI variations in the last period of observation: the fleet fatigue behaviour of the last period is very close to previous one, within a variation of ±3%. The fleet typically performs flights of a duration shorter than design and at a higher altitude than design mission profiles.

2.5 M-346 In-Service Monitoring (Leonardo Aircraft Division)

The M-346 has been selected by several countries to serve as an advanced trainer for their pilots; 85 aircraft are currently in service, with major customers including the Italian Air Force (ItAF) with 22 aircraft, including 4 aircraft operated by the International Flight Training School (IFTS), the Israeli Air Force (IAF) with 30 aircraft, and the Republic of Singapore Air Force (RSAF) with 12 aircraft.

M-346 Advanced Trainer implements a Health & Usage Monitoring System (HUMS) that enables monitoring and data collection of on-board equipment and of airframe structure.

Data analysis method, based on a non-parametric statistic, allows actual aircraft spectra usage being investigated for each customer (but the approach is also applicable to other parameters). Results (see Figure 2.6 for typical examples) provide an evaluation in terms of safety, maintenance costs, and inspection plan of customer fleet based on real usage (and not on design usage).

Data about customer usage spectra increases Leonardo Aircraft know-how that will be available for future projects.

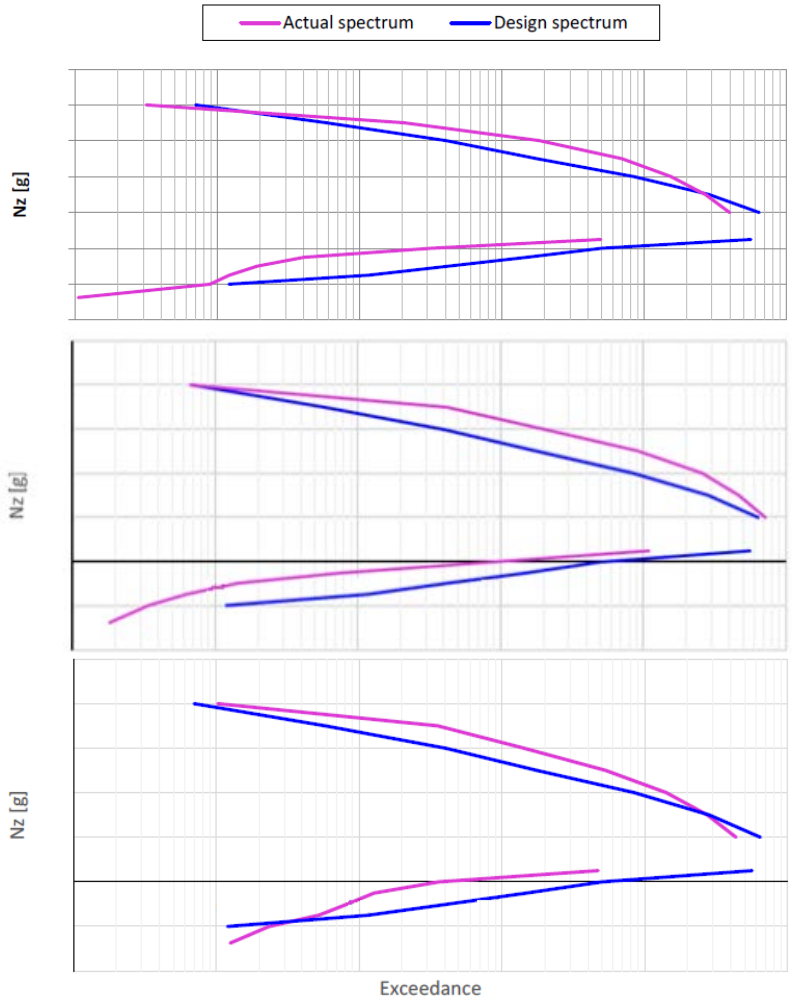

Figure 2.6 Non-dimensional Real Nz spectrum of different M-346 fleets: RSAF top, IAF mid, and ItAF+IFTS bottom.

2.6 Rotorcraft Usage Monitoring through Machine Learning (Leonardo Helicopter Division)

Helicopter maintenance plans are normally defined on the basis of expected (design) mission profiles, that may be quite different with respect to the actual scenario in which the helicopters will operate. The definition of an improved maintenance plan can be achieved through a periodical validation of the initial usage hypothesis, that can confirm or suggest proper amendments so to develop diversified Maintenance Plans tailored to the actual usage of every specific fleet (the so-called Effective Maintenance Plans).

Benefits expected by such an approach, sketched in Figure 2.7, are the evolution from Time-Based Maintenance (TBM) to Condition-Based Maintenance (CBM), a reduction of Maintenance Costs which are a substantial portion (≈ 25%) of Direct Operating Costs, and an increase of Flight Safety.

An Effective Structural Usage Monitoring (ESUM) is possible only if an effective and reliable Flight Condition Recognition (FCR) is available. An essential requirement for such a system is the capability to analyse automatically and swiftly large data sets registered by a fleet of 'Family' helicopters, such as AW169, AW139 and AW189 (about 100 hours per month per aircraft flown).

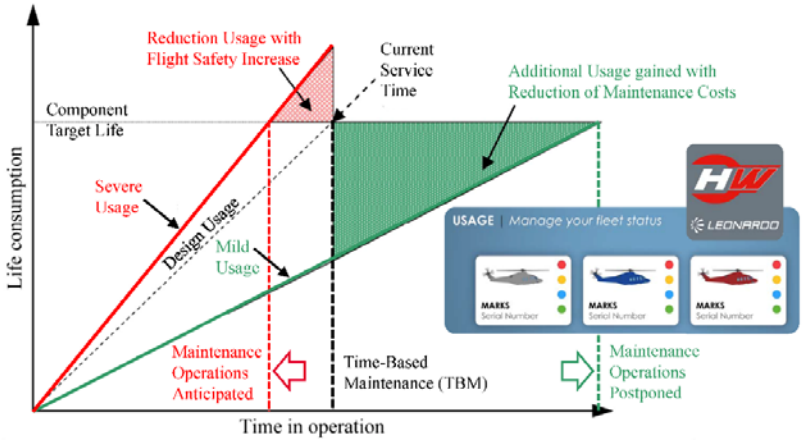

Figure 2.7 Real usage and Condition Based Maintenance

A research programme has been developed, in cooperation with two Departments of Milan Polytechnic (Department of Mechanical Engineering and Department of Electronics, Information and Bioengineering), with the purpose of developing an advanced software tool, capable to provide an automatic, reliable, and efficient analysis of the time histories of the principal usage parameters recorded on board during flight operations. A new Flight Conditions Recognition (FCR) algorithm has been developed adopting a combination of Machine Learning (M/L) approaches, which are particularly suitable for the analysis of massive data set structures (Big-Data). The logic of the approach to Flight Conditions Recognition is explained in Figure 2.8. The data "lake" is composed of the time sequences of the principal flight parameters recorded by the HUMS fitted on board.

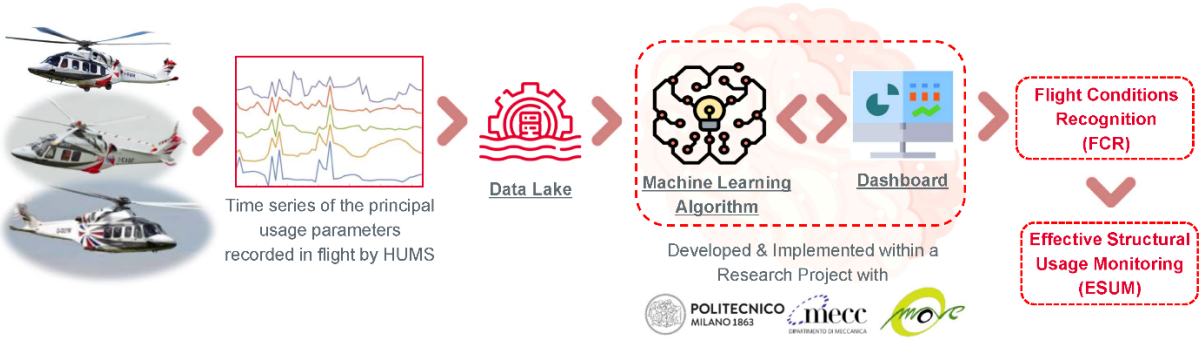

Figure 2.8 Logic of the Flight Conditions Recognition analysis software.

To develop the ML Algorithm a specific Dataset of Load Survey Flights composed by Labelled Manoeuvres has been used (see Table 2.1 for info about number of flights and manoeuvres employed for each of the helicopters in the AW Family). Three fourths of the dataset have been used for Training the Supervised ML Algorithm while the remaining flights and manoeuvres have been devoted to Testing & Verifying.

	Helicopter Model		
	AW 189	**AW 169**	**AW 139**
Number of flights	207	220	598
Number of manoeuvres	4673	4652	8068

Table 2.1 AW – Family Products data sets used for developing the ML Algorithm.

The major challenge of the activity is related to manoeuvre recognition, because of the inherent differences in duration and loading factor that can be ascribed to piloting techniques and to the

environment. An additional issue related to manoeuvres is their combination, which may occur in practice when two manoeuvrers are executed contemporarily.

A rebalancing procedure of the dataset has been developed to improve the performance of the Machine Learning (ML) algorithm. Dataset rebalancing is organised in two steps: a first step that aggregates manoeuvres with similar characteristics into Macro-categories and a second step that identifies single Flight Conditions inside the macro-categories via deterministic features (see Figure 2.9)

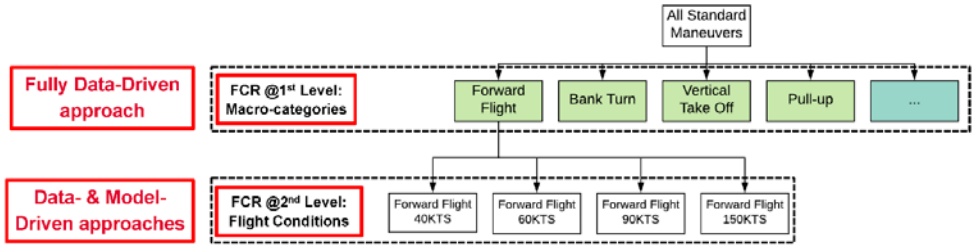

Figure 2.9 Dataset Rebalancing through Aggregation.

Since the data set for training the system cannot cover all combinations, statistical features are extracted analysing the time histories by means of “sliding windows” and two strategies employed to elaborate predictions; finally, a supervisor algorithm chooses the best option (*Figure 2.10*).

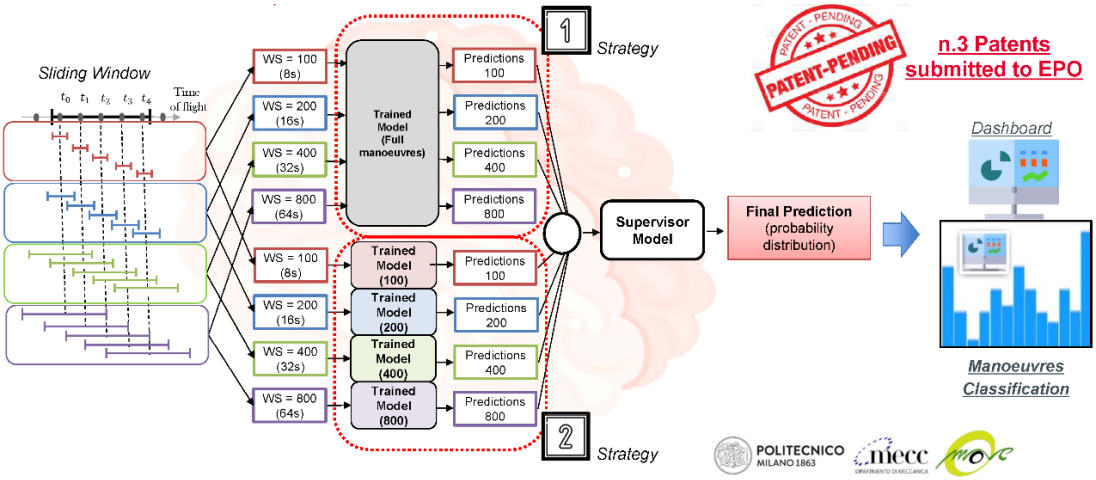

Figure 2.10 Machine Learning (M/L) Algorithm – from Time Histories to Statistical Features for Training phase.

The Dashboard permits to visualize the results of the M/L Algorithm in terms of classified manoeuvres in both a detailed (Flight Explorer) and an aggregated (Helicopter Explorer) way (*Figure 2.11*).

The Flight Explorer environment offers detailed Information at Flight Level such as the trends of the flight parameters recorded by HUMS (Flight Parameters Visualizer) or the way each flight is segmented into manoeuvres (Flight Segmentation Visualizer).

The Helicopter Explorer environment shows aggregated information such as the amount of time spent in every recognised manoeuvre by a specific helicopter of the fleet, or the number of occurrences of any manoeuvre for a particular helicopter.

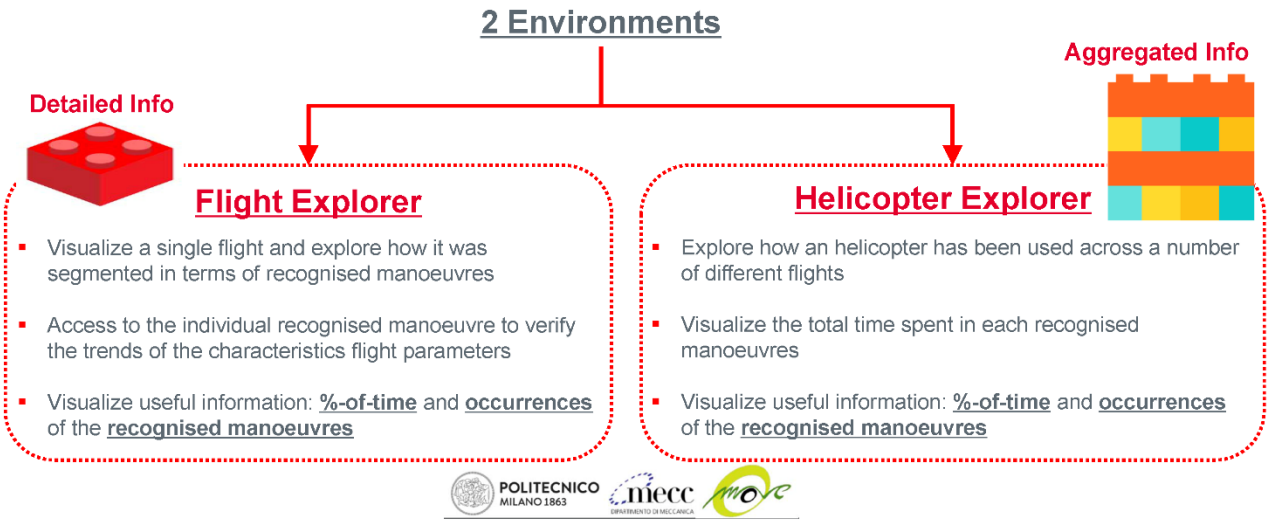

Figure 2.11 Dashboard – Front End interface.

2.7 Export Eurofighter aircraft – New setting of BSD recording start

Prior to delivery to final customers, the export version of the Eurofighter aircraft undergoes a series of Production Flight Acceptance Testing (PFAT) flights during which flight parameters are recorded on the on-board Bulk Storage Device (BSD). The recording of parameters begins as soon as the brake speed on ground is exceeded.

Currently, this speed is set at 1.5 m/s, which causes parameter recording to start as soon as the aircraft leaves the parking area. The problem arises for some PFAT flights during which the aircraft stops, after leaving the parking area, to perform the on-ground checks/failure resolution of the E-Scan radar. This activity can take several minutes and, due to the memory limitations of the BSD, can result in the loss of data relating to the final phases of the flight.

A new brake speed on ground must then be defined, against which the parameter recording during the PFAT flights will be started.

Leonardo has carried out an evaluation, from the fatigue point of view, that defines the relative damage of the most stressed location during the on-ground phase as a function of the speed at which the BSD recording starts. Such analysis allows one to determine the extent of the relative damage that is neglected when considering the new setting of the speed for BSD recording to start.

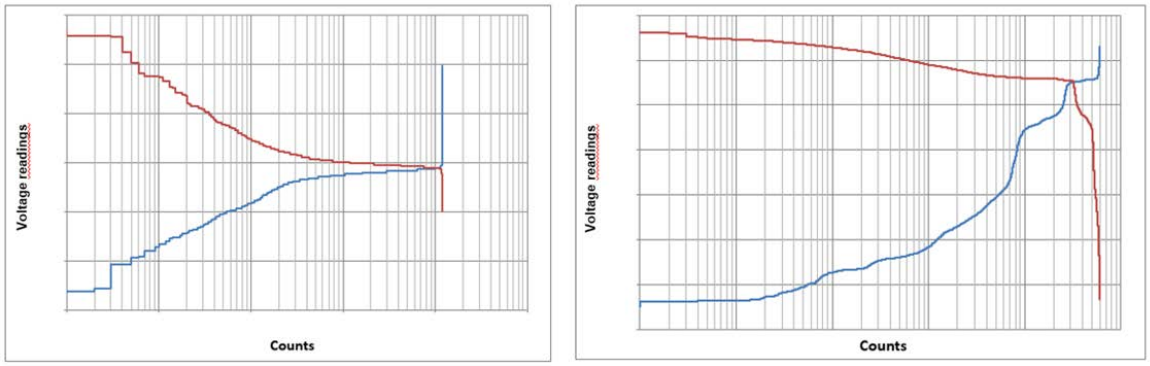

Figure 2.12 Stain Gauge #1 reading spectra: ground phase (left) and total flight (right).

The first step of the study is based on defining which Strain Gauge (SG) location has the higher relative damage during the on-ground phase of the flight. The on-ground phase starts at the initial registration speed (1.5 m/s) and ends when the maximum take-off speed is attained.

Rainflown has been performed on the SG readings for both the whole Flight and the on-ground phase to obtain the spectra shown in Figure 2.12 (relevant to SG #1). Through this process the relative damage of all single SG (except for location #5, #11 and #16) could be defined. The relative damage is the damage of the on-ground phase compared to that of the whole flight.

In the second step the relative damage relevant to the time interval between the initial BSD recording speed (1.5 m/s) and the hypothetical one chosen as new point for starting BSD recording was calculated.

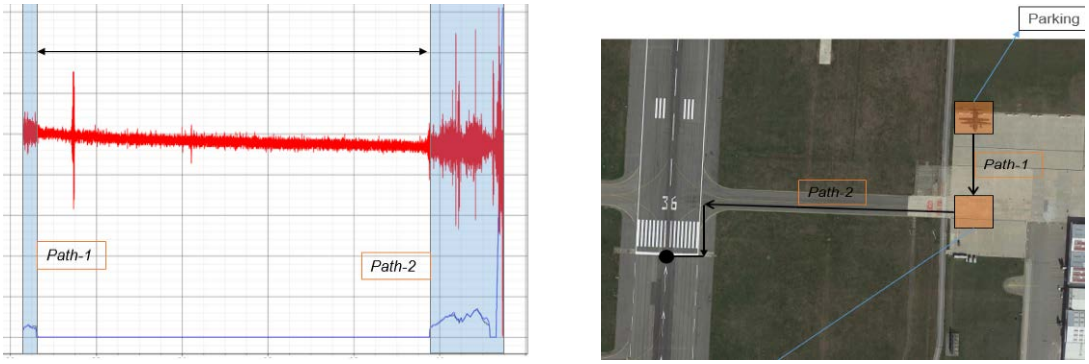

Figure 2.13 Split of ground phases in several paths.

In this way the E-Scan radar checks phase can be omitted, and a considerable number of minutes saved (Path-2 in Figure 2.13).

From the investigation the following evidence has arisen (see Figure 2.14):

- Strain gauge location 1 has the highest life consumption for the on-ground phase.
- The relative damage is already negligible considering the strain gauge readings between the start recording of parameters (1.5 m/s) up to the achievement of 10 m/s speed.

Eventually, from the results obtained, and adding some conservativism to the estimates, the relative damage calculated considering the strain gauge readings until reaching a 7 m/s speed can be considered negligible.

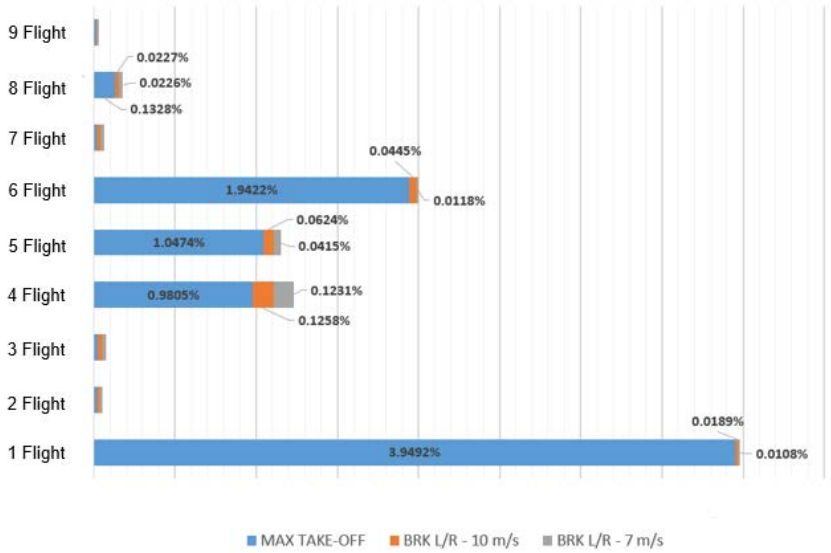

Figure 2.14 Relative Damages from S/G number 1.

3 METALS

3.1 Fatigue behaviour of notched and un-notched materials

3.1.1 Unique Materials for Advanced Aerospace Applications – UMA3 (University of Bologna)

The University of Bologna – Forlì Campus is participating to a Horizon 2020 aerospace-oriented EU project titled Unique Materials for Advanced Aerospace Applications (UMA3). The overall aim of the project is to build a value chain consisting of research institutions that are involved in studies on powder metallurgy processes, additive manufacturing, surface technology and fully 3D investigations.

Within the UMA3 project, the goal of the University of Bologna unit is to investigate the use of powder metallurgy and additive manufacturing technologies to provide new solutions for the aerospace industry. In particular, the objective is to study the mechanical behaviour of light alloys components, made by powder metallurgy and additive manufacturing. To this aim, the following steps are under investigation:

- Production of high-performance Al-alloys specimens manufactured by Powder Metallurgy (PM) and Additive Manufacturing (AM).
- Comparison of the mechanical properties of PM & AM samples.

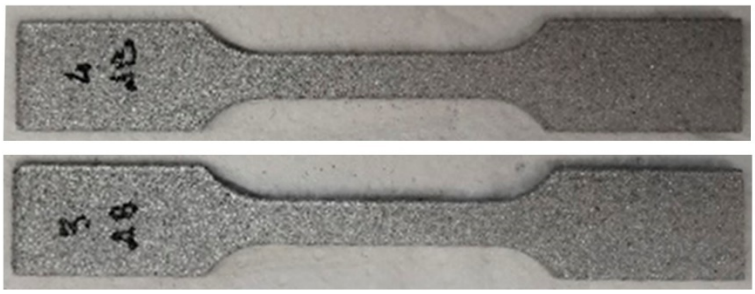

Figure 3.1 Al-Sc coupons produced by Laser Powder Bed Fusion.

The selected material is a new Al-Sc alloy (Scalmalloy) with high performances. Flat dog-bone specimens have been produced by Laser Powder Bed Fusion (L-PBF) in Bologna laboratory (see Figure 3.1). Two batches of specimens have been tested: as-built (AB) and heat-treated (HT – 325°C for 4 hours).

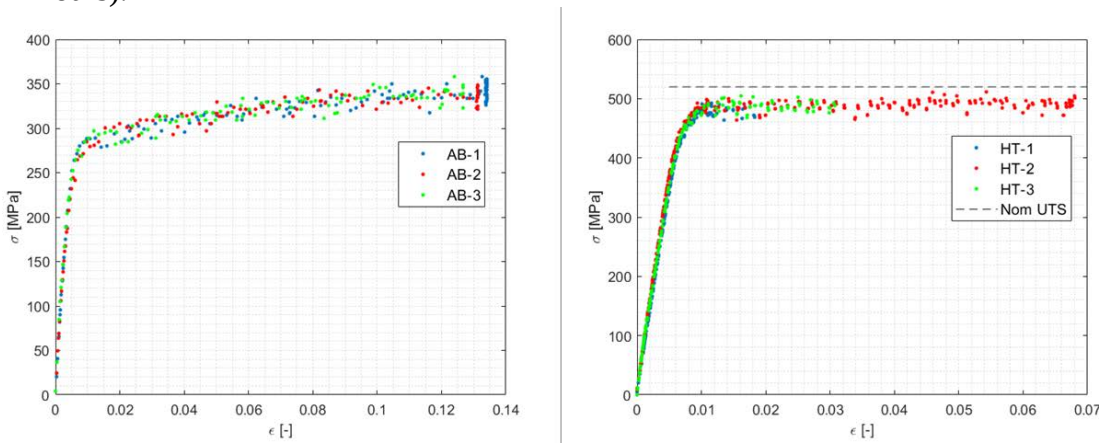

Figure 3.2 Al-Sc tensile test results for As Built (AB) and Heat-Treated (HT) specimens.

Preliminary testing under quasi-static loading conditions have been carried out to assess the ultimate strength and surface hardness and evaluate the effect of the heat-treatment.

The average UTS of the untreated samples is about 350 MPa (see Figure 3.2, left side), while that of the heat-treated samples is about 490 MPa, approximately 6% lower than the nominal value reported for Scalmalloy, namely 510-530 MPa (see Figure 3.2, right side). These values agree with recent literature.

Further tests under fatigue loads are ongoing. The outcome of this work is to contribute to the characterisation of the microstructural and mechanical properties of components produced by powder metallurgy, which is a fundamental step towards their application alongside components produced by conventional techniques.

3.1.2 REACH regulation implementation (Leonardo Aircraft Division)

In recent National Reviews, information was given about an experimental program, in progress at Leonardo Aircraft Division, for the assessment of the influence of protective treatments, compliant with the current international environmental regulation (**REACH** – **R**egistration, **E**valuation, **A**uthorization and Restriction of **Ch**emicals), on the fatigue behaviour of the most common metallic alloys. Leonardo Aircraft Division has carried out several research activities with the aim of replacing different metal surface protection processes based on hexavalent chromium with more ecological ones, performed using trivalent chromium products.

Thermal Spray Coatings for replacing the Hard Chromium Plating process

Hard chromium plating is used on steel alloys for increasing surface hardness, improving the wear and friction resistances, improving corrosion behaviour for non-corrosion resistant substrates, decreasing the friction coefficient, and preventing galling between metallic materials.

To satisfy the REACH regulation, alternative processes based on Thermal Spray Coatings are being investigated, developed, and qualified, to be used on steel alloys in place of the Hard Chromium Plating.

Thermal sprayed metallic coatings are produced by projecting the molten coating metal by mean of a stream of gas or plasma, onto the surface to be coated. Such coating is performed by several passages, each one depositing a layer of about 20 μm by piling up “splats” on a substrate surface. Since the gases are accelerated to supersonic speed, and oxidation occurs, the process is also called High Velocity Oxi Fuel (HVOF).

The fatigue test campaign has determined the fatigue behaviour of selected steel alloys subjected to both Hard Chromium and HVOF process. Although steel is not widely used for significant structural items, Leonardo proprietary programs have been reviewed and the most representative steel materials have been selected: AISI 4130 and 15-5PH, both in sheet form. Fatigue behaviour has been also investigated for the same materials without any surface protection to estimate the HVOF treatment correction factors on basic fatigue properties.

The test campaign has been completed and 60 specimens have been tested. The results show that HVOF process does not adversely affect the fatigue characteristics compared to the Hard Chromium process.

Zinc-Nickel Plating for replacing Cadmium Plating

To comply with the REACH regulation Zinc-Nickel Plating of steels alloys has been investigated to replace the Cadmium Plating Process. To assess the impact of the new coating process on fatigue behaviour, Leonardo carried out a fatigue test campaign on the most used steel alloys in proprietary programmes: AISI 4130 and INOX 15-5 PH. The test campaign has been completed during which 80 specimens have been tested. Fatigue behaviour of untreated specimens has been evaluated to estimate the correction factors to apply to basic fatigue properties.

Test results led to conclude that the Zinc-Nickel plating process does not adversely affect the fatigue characteristics compared to Cadmium plating process. In fact, the ratio between Zinc-Nickel and Cadmium plating fatigue allowables is always higher than 1.0, so it can be concluded that, as far as fatigue aspects are concerned, the Zinc-Nickel plating can replace the Cadmium plating without any limitation.

3.1.3 Testing of Additively manufactured Aluminium Alloy (Leonardo Aircraft Division)

A test campaign has been organized by Leonardo Aircraft Division to estimate the fatigue behaviour of the Additive Manufacturing (AM) fabrication process. Specimens have been fabricated from Al Alloy powder (AlSi10Mg) in different configurations for carrying out fatigue, crack propagation and toughness tests. In particular specimens with different structural and geometrical features (i.e. open hole, notch, joint, countersunk) were fabricated also varying some of the process parameter (roughness, laser overlap, fabrication direction). Notched tensile and open hole specimens, lugs and joints were tested. An example of the tensile AM specimen is shown in Figure 3.3; in the same figure, the typical surface quality obtainable with the technology is shown.

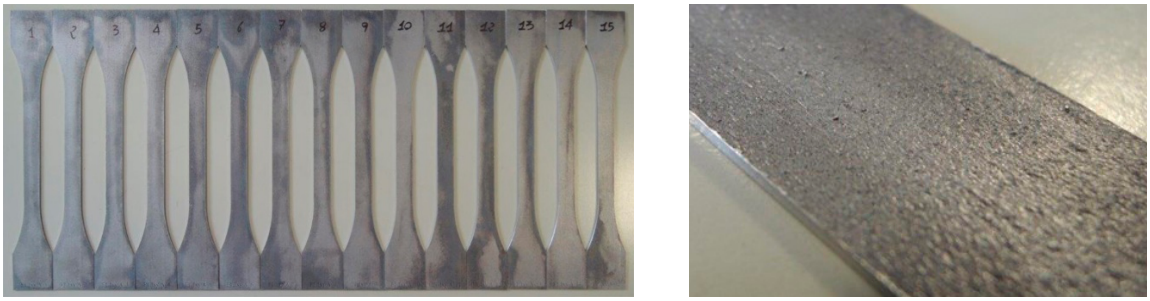

Figure 3.3 Example of Additively manufactured Aluminium Alloy specimens.

The fatigue behaviour at different Kt is unpredictable, for example, the allowable at Kt=3 is greater than the one at Kt=2. Moreover, the well appreciable gap between curves at Kt=1.05 and Kt=3 of the AA2024-T3 alloy is not the same observed for the corresponding curves obtained for specimens produced by mean of the Additive Manufacturing process, that are very close to each other. Also, the behaviour at different roughness levels is quite similar, while a greater influence of such parameter was expected.

A possible explanation could lie in the anomalies of the internal structure of the material that may affect considerably the fatigue behaviour. Due to the dispersion of the results, the positive effects of the fabrication direction are not clearly appreciable, so a preferred fabrication direction is not easily established.

Based on the data obtained, the technological process does not seem mature enough for manufacturing main aircraft structural components. To better understand the results obtained, a campaign of metallographic investigations is foreseen for all those specimens that exhibited anomalous duration and premature failure.

The current fatigue performance of additively manufactured specimens is influenced by the stratification and depends on the direction of grains, the surface finishing and roughness, and the flatness of specimens. Possible improvements to the material properties could be achieved by the addition of a specific post-production heat treatment.

3.1.4 Testing of laser cut parts (Leonardo Aircraft Division)

The Laser cutting process of sheet metal alloy allow efficiency and velocity in production while ensuring both flexibility and accuracy in cutting. Notwithstanding its indubitable advantages, the presence of the so-called Heat Affected Zone (HAZ) requires reworking to eliminate it from

primary aeronautical components, such rework implies time and costs that limit the application of the Laser Cutting process in aeronautics.

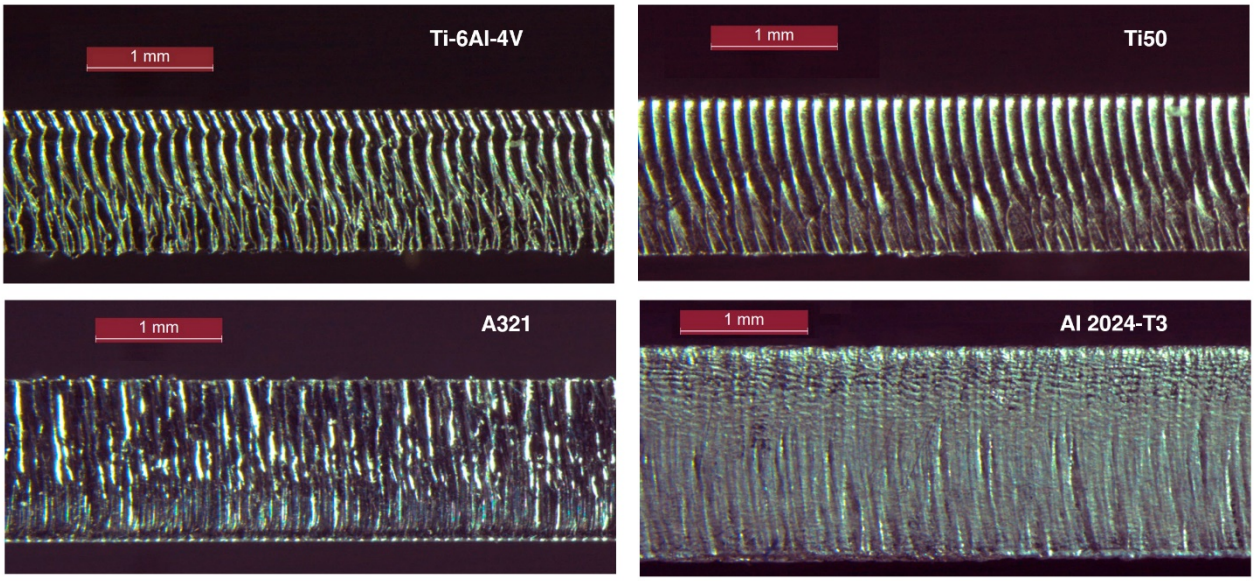

Figure 3.4 Laser cutting typical edge quality for different material.

Leonardo Aircraft Division has investigated the effect of HAZ on the fatigue behaviour to evaluate the possibility to apply the process without removing the HAZ zone.

The fatigue test campaign has been carried out on selected Aluminium, Titanium and Steel alloys: they are Al 2024-T3, Ti50, Ti-6Al-4V and A321. Edge quality obtainable with the laser cutting is shown in Figure 3.4 for the selected materials. The results allow the fatigue behavior of the laser cutting process to be compared to that of the conventional mechanical cutting process.

About 200 specimens have been fabricated and fatigue tested. For Al 2024T3, A321 and Ti50 materials, no significant differences in terms of fatigue behaviour have been obtained between the mechanical and the laser cutting processes. For the Ti6Al4V material, probably due to its peculiar mechanical properties, a not negligible fatigue knockdown factor has been obtained.

3.1.5 One-up drilling process (Leonardo Aircraft Division)

One-Up Assembly (OUA) is a term that applies to joints that are specifically exempted by engineering authority (data set or drawing), or by the applicable specification(s), from the requirement to clean and/or deburr holes prior to fastener installation.

Leonardo Aircraft Division has planned a test campaign to evaluate the fatigue knock-down factors for one-up drilled hybrid (metal-composite) joints containing aluminium and titanium elements.

One-Up Drilling of hybrid Aluminium–Composite joints

Three kinds of hybrid Aluminium–Composite joints have been tested to determine the trend of the knockdown factor with the transferred load. Specimen types differ in terms of transferred loads and include the open hole geometry as the zero-load transfer joint. Example of the specimens' geometries tested are shown in Figure 3.5.

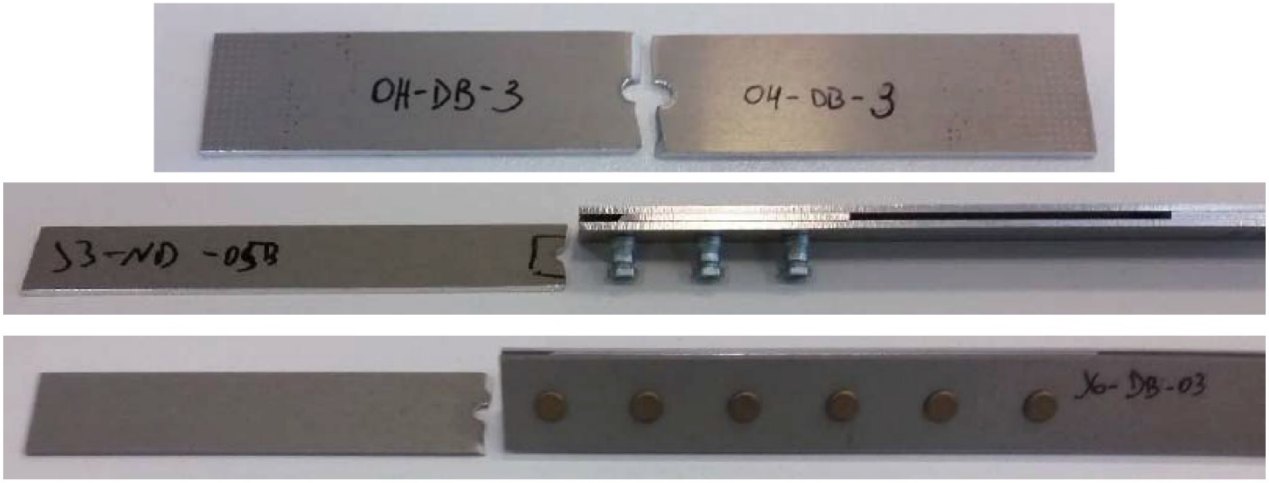

Figure 3.5 Examples hybrid Aluminium–Composite joints for One-Up Drilling.

For each one of the above-mentioned geometries, specimens with deburred and non-deburred holes have been manufactured and tested. in which The specimens have been grouped according to the burr height ranges, as shown in Table 3.1.

Group A [µm]	Group B [µm]	Group C [µm]	Group D [µm]
110 - 129	139 - 150	156 - 170	188 - 206
100 - 120	133 - 150	160 - 173	186 - 208
100 - 123	134 - 150	160 - 174	187 - 207

Table 3.1 Grouping of Aluminium–Composite specimens according to the range of burr height.

The engineering evaluation of the results has been completed and the analyses, relevant to aluminium-composite assembled parts, have shown fatigue performances to be quasi-independent on the burr height in the range considered (deburred up to 208 µm). All the fatigue knockdown factors are very close each other, so for burr heights up to 200 µm a common factor can be used.

One-Up Drilling of hybrid Titanium–Composite joints

As it has been done for hybrid Aluminium–Composite joints, three kinds of hybrid Titanium–Composite joints have been tested to determine the trend of the knockdown factor with the transferred load, the metallic parts have been manufactured in Ti6Al4V alloy.

Group A [µm]	Group B [µm]	Group C [µm]	Group D [µm]
63 - 100	101 - 137	150 - 180	184 - 219
60- 100	101 - 138	142 - 178	182 - 213
60 - 98	101 - 135	146 - 179	181 - 218

Table 3.2 Grouping of Titanium–Composite specimens according to the range of burr height.

Specimen types differ in terms of transferred loads and include, also in this case, open hole specimens as the zero-load transfer joint. For each geometry, specimens with deburred and non-deburred holes have been manufactured and tested. The specimens have been grouped according to the burr height ranges, as shown in Table 3.2.

Tests on 150 specimens have been completed and engineering evaluation of results has been performed.

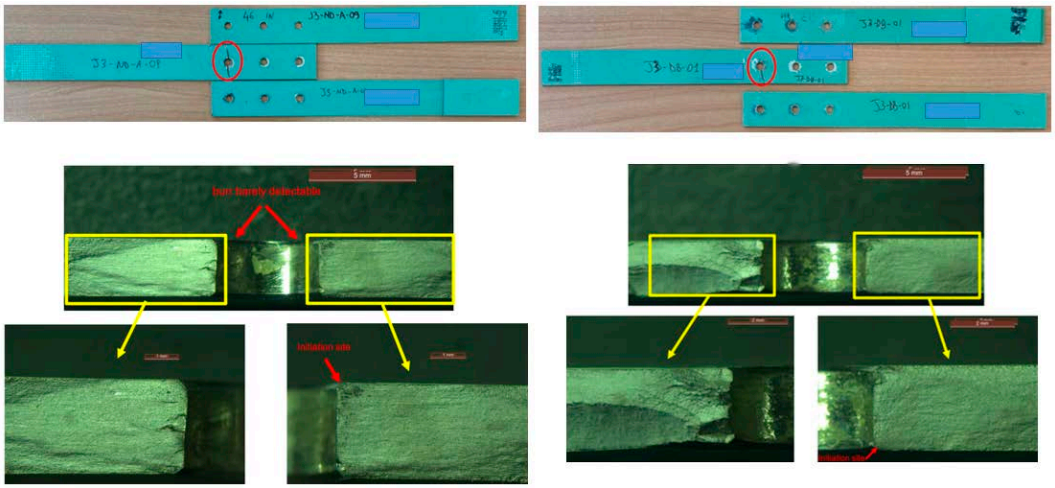

Figure 3.6 Deburred (DB) and Non-Deburred (ND) Titanium J3 Joint specimens.

For J3 (see Figure 3.6 for an example) and J6 joints similar results were obtained for burr height up to 220 μm; fatigue behaviour has been found independent of burr height and no fatigue knockdown factor is necessary for such configurations. For OH specimens (Figure 3.7) some differences have been found but their interpretation is not certain and additional tests are planned to better investigate this phenomenon. An additional test campaign on Filled Hole specimens without load transfer shall also be performed.

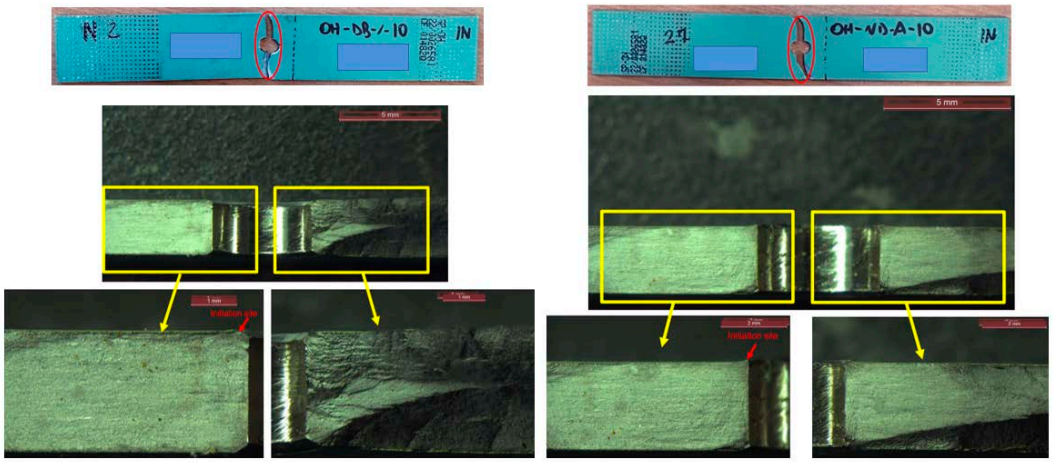

Figure 3.7 DeBurred (DB) and Non-Deburred (ND) Titanium Open Hole specimens.

3.2 Crack propagation and fracture mechanics

3.2.1 Fracture tests of friction stir welded plates machined from forged AA 2219-T851 shells (Univ. Pisa)

The University of Pisa carried out an experimental program, in collaboration with Thales Alenia Space Turin, aimed at assessing the fracture behavior of Friction Stir Welded flat plates machined from plate and/or forged AA 2219-T851 shells. The tests were carried out on three groups of

specimens. The first group of specimens (prefix FF) was obtained by Friction Stir Welding plates machined from forged AA 2219.

The second group (prefix PP) was obtained by Friction Stir Welding AA 2219 plates while the third group (prefix PF) was obtained by Friction Stir Welding a plate machined from forged AA 2219 to a standard plate of the same material. Five additional plate-to-plate specimens, joined by means of a double pass process, representative of a repair welding, were tested for a total of 31 tests.

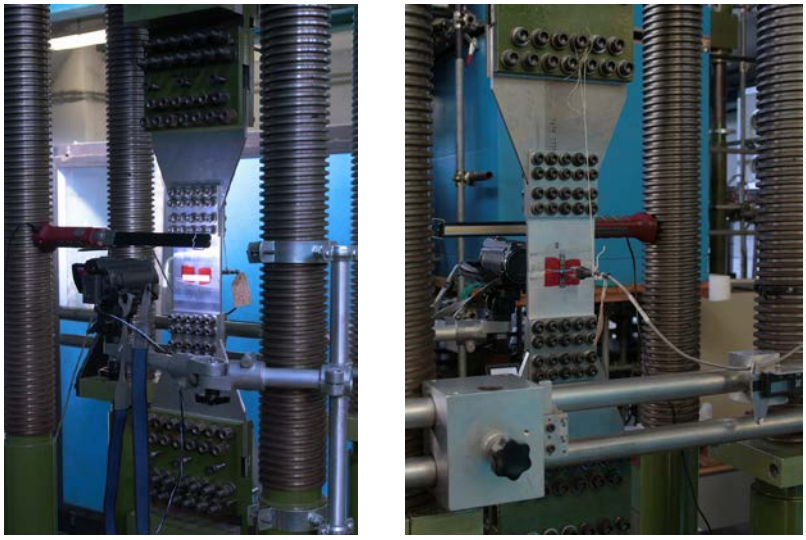

Figure 3.8 FSW fracture tests: test set-up

For each group, two different positions of the starting notch were considered: at nugget centre and in the retreating Thermo-Mechanical Altered Zone (TMAZ). Start notches in the form of a through-crack were manufactured about 3 mm shorter than the required initial crack dimensions, to allow fatigue pre-cracking.

All the tests were performed on a servo-hydraulic fatigue machine with 200 KN maximum load capacity. The machine was equipped with special grips, developed during a previous test campaign, to test 100 mm wide specimens with short lengths (150-200 mm).

After pre-cracking the specimens were subjected to a fracture test. In this phase, the specimens were instrumented with a clip gauge, to measure the crack opening displacement. The test set-up is shown in Figure 3.8.

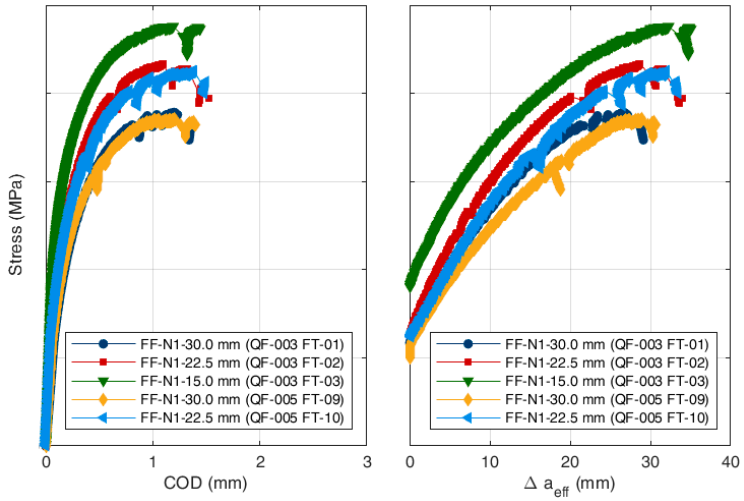

Figure 3.9 gross stress evolution with COD and crack extension

Prior to test, each specimen was pre-cracked by applying constant amplitude fatigue load, with a stress ratio R = 0.1; crack growth has been monitored by means of a high-resolution microscope.

The fracture tests were performed at constant rate displacement (approximately 0.3 mm/min). The tests ended with specimen failure, or, when an unsteady increase in the crack length occurred, with a consequential drop of the load. Both the crack propagation and the crack-extension resistance tests were performed at room temperature.

Load, displacement of the mobile grip and crack opening displacement were digitally recorded during the tests. The R-curves and the stress intensity factors were derived by elaborating load and crack opening displacement data according to the procedure recommended in ASTM E 561.

An example of the evolution during the test of the gross stress with both COD and calculated effective crack extension is shown in Figure 3.9 for group FF, nominal welding process (N) process with centre crack (Type 1). The R-curves for same group are plotted in Figure 3.10; the open symbols points indicate the critical condition.

Taking PP specimens as a reference the following results, in terms of engineering fracture toughness, have been obtained:

- FF specimens have a comparable fracture toughness. FP specimens obtain similar results.
- The position of the initial crack shows negligible influence.
- The double pass repair process shows a minor effect on toughness.

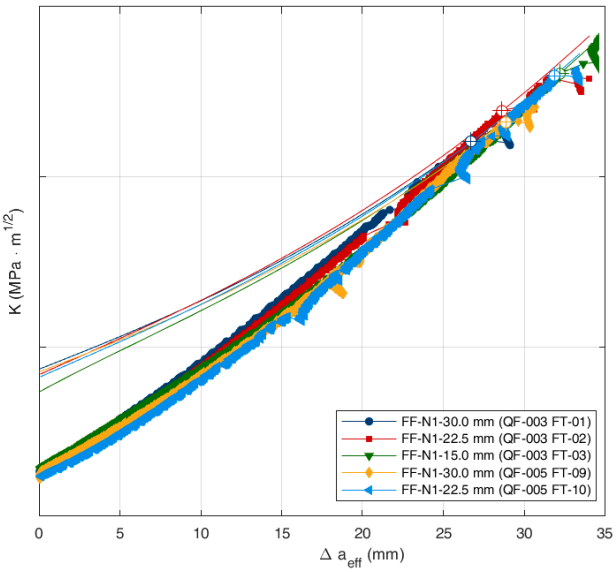

Figure 3.10 R – curves (crack extension resistance vs effective crack increment)

3.3 Corrosion and fatigue

3.3.1 Corrosion Effects Assessment on Fatigue Behaviour of Al 7475-T7351 (Leonardo Helicopter Division)

A joint research project between Leonardo Helicopter Division and the Departments of Mechanical and Chemical Engineering of Polytechnic of Milan has been set up to verify the equivalence of the flaw tolerance behaviour of defects, with the same transversal dimension (expressed in terms of $\sqrt{Area}$), produced by electro-erosion and by different corrosion processes. Electrochemical attack (A1) and Salt spray exposition (A2) have been considered as Artificial and accelerated corrosion processes, while exposition to Urban environment (N1) and Marine environment (N2) have been selected as Natural corrosion processes.

The objective of the research is the evaluation of the threshold of non-propagation of small cracks, like defects, used to build the Kitagawa diagram and its application domain, in 7475-T7351 Aluminium Alloy. Such material has been chosen first since it is typically used for helicopter dynamic parts.

The research program is part of Leonardo HD effort for the European Plan for Aviation Safety 2020-2024 on 'ageing of the fleet' and some preliminary results have already been presented in the previous edition of the National Review.

The first group of tests, that also constitute a reference for comparison with subsequent results, has been carried out on EDM specimens with R=0.1. The Staircase (Hodge-Rosenblatt) method is used to define the endurance limit, and the test is considered a "Run-Out" if it survives 10^7 fatigue cycles. For such group of specimens, a target transversal dimension of 0.445 mm has been selected to harmonize the results of fatigue tests with those of a previous activity performed on Micro-notched specimens. SEM images of both a typical EDM defect and of a micro-notch are shown in Figure 3.11, while a comparison of fatigue limit for specimens containing the two types of defects is shown in Figure 3.12.

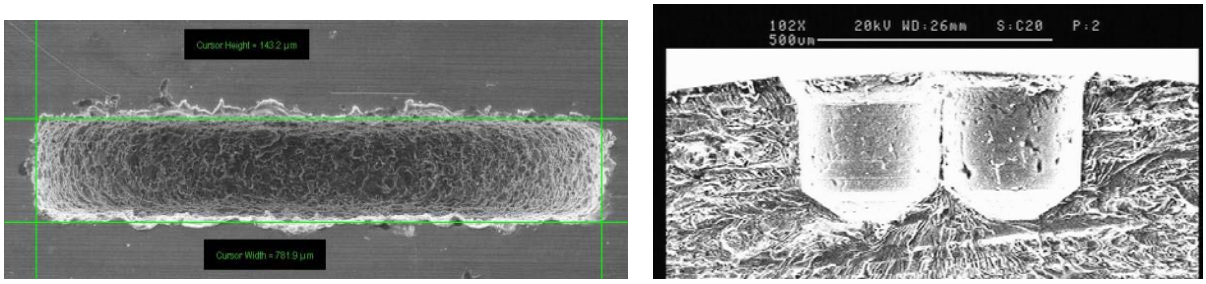

Figure 3.11 SEM images of an EDM defect (on the left) and of a Micro-notch (on the right).

.

For the other groups the following applies.

Electrochemical Attack – Galvano-static procedure (A1)

A Galvano-static procedure has been "*ad hoc*" designed for promoting a localized corrosion pit with geometric characteristics similar to those of EDM specimens, with a target $\sqrt{Area}$ of 0.445 mm. The procedure has been applied to 25 specimens for a 10 hr 8 min duration time (*from Faraday's Law*); then the specimens have been examined to characterize the shape and depth of the defect, so comparisons with the other types of damages could be made.

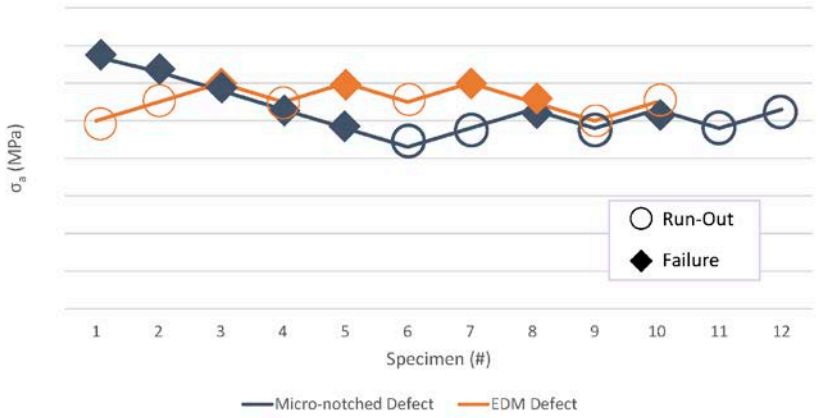

Figure 3.12 Comparison of fatigue limit for the specimens containing the two types of defects.

A subset of 12 specimens, electrochemically corroded through the Galvano-static procedure, has been selected for similarity with the EDM specimens' defect, adopting the criterion of minimizing the discrepancy of the mean √Area. The selected 12 corroded specimens have been subjected to the Stair-case sequences to identify the fatigue limit at 10^7 cycles and stress ratio R=0.1. The results are shown in Figure 3.13 (in grey), together with those belonging to EDM and micro-notch specimens (already presented in Figure 3.12); a similarity in results can be observed.

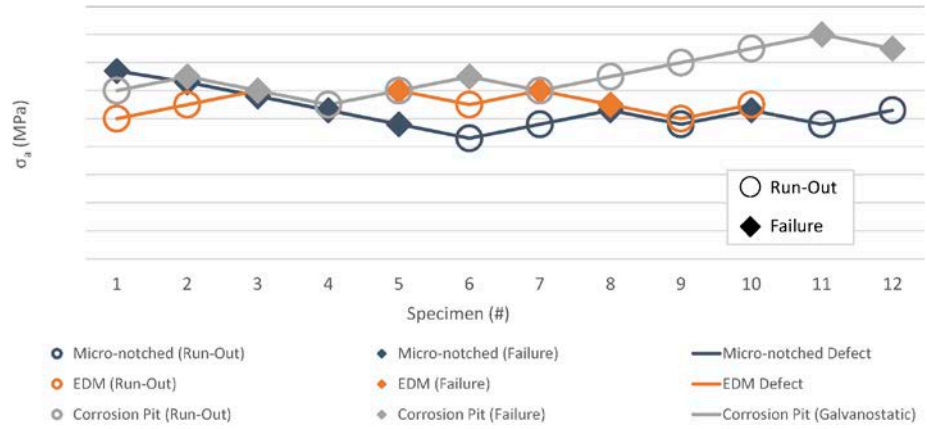

Figure 3.13 Comparison of fatigue limit for the Galvano-static corroded specimens.

Salt Spray exposition (A2)

Following *ASTM B117 – Standard Practice for Operating Salt Spray*, 25 specimens have been subjected to Salt Spray exposition for 1 month and then fatigue tested following the same procedure of the previous series. A subset of 10 artificial corroded specimens through the Salt Spray procedure has been selected for similarity with EDM specimens' defect.

Fatigue testing has been carried out at constant amplitude with R=0.1 as for previous sets. The results are shown in Figure 3.14 (in yellow). A close similarity to results belonging to EDM and micro-notch specimens can be detected.

Urban environment exposition (N1)

To evaluate the corrosion effects of a "natural" urban environment 15 specimens were exposed outdoors in Milan and were monitored monthly for one year.

The activity evidenced only negligible corrosion pits (a few microns) so it was decided to avoid fatigue testing the specimens.

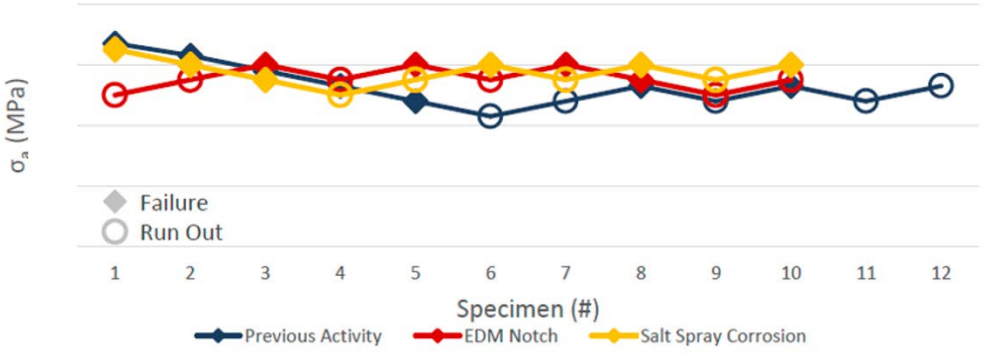

Figure 3.14 Fatigue limit for specimens corroded via Salt Spray exposition.

Marine environment exposition (N2)

To evaluate the corrosion effects of a "natural" marine environment 15 specimens were exposed outdoors, near the sea, in the town of Bonassola (SP) and were monitored monthly for one year.

As for the other sets, fatigue testing has been carried out at constant amplitude with R=0.1 following the Staircase (Hodge-Rosenblatt) method to define the endurance limit.

The results are shown in Figure 3.15 (in grey); it is evident that the corrosion Hot spots result to be less severe in terms of Dimensions compared to the ones produced by the Artificial procedures.

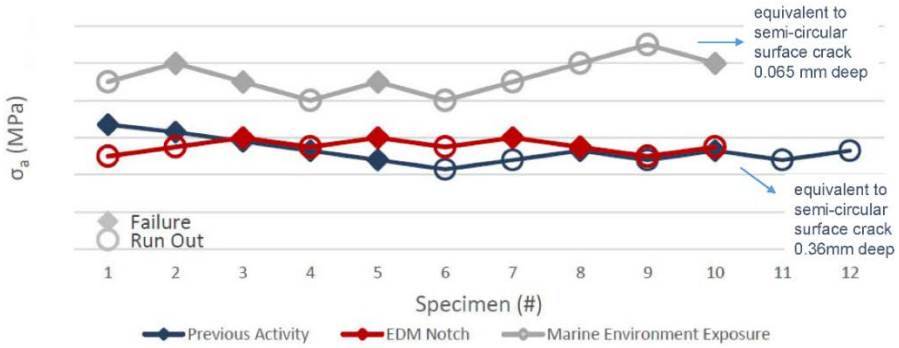

Figure 3.15 Fatigue limit for specimens corroded in a "natural" marine environment.

Comparison of endurance limit test results for different types of defects in 7475-T7351.

A graphical comparison of endurance limit test results for the different types of corrosion defects in 7475-T7351 is shown in Figure 3.16

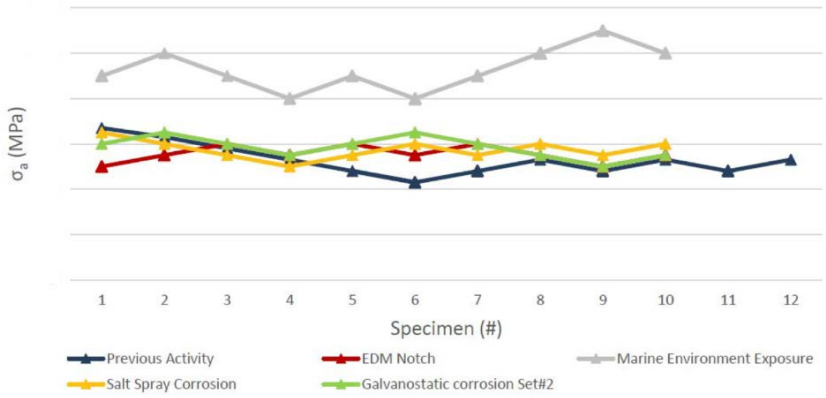

Figure 3.16 Comparison of fatigue limit for results for the different types of corrosion defects

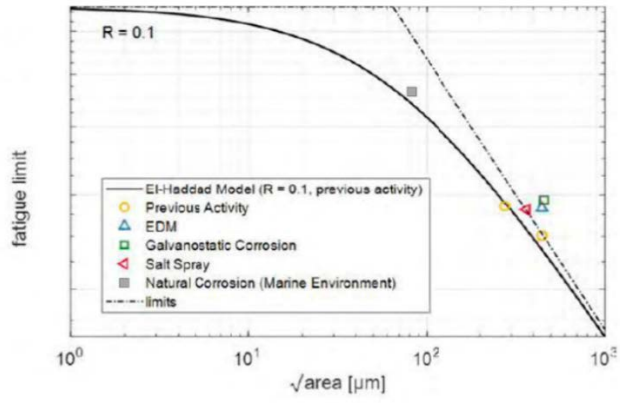

Figure 3.17 Fatigue limit vs flaw transversal dimension for the different types of corrosion.

All the results are in line with the theorical behaviour foreseen by the Kitagawa Model for the fatigue strength reduction due to micro-defects as shown in Figure 3.17.

3.4 Structural Health Monitoring

3.4.1 Structural Health Monitoring – Acoustic Emissions (Univ. Bologna)

Structural Health Monitoring (SHM) is a key technology enabler for the long-sought shifting from a time-based to a condition-based maintenance of aircraft structures. In this context, Acoustic Emission (AE) is a promising technique for the monitoring of large areas by analysing Lamb Waves propagating in plate like structures.

To reconstruct an original and unaltered signal from an AE event, a novel Time Reversal (TR) methodology has been developed at the University of Bologna – Forlì Campus, and preliminary results have been reported in the previous edition of the National Review. The novelty of the method consists in the use of a Frequencies Compensation Transfer Function (FCTF) to reconstruct Broad-Band (BdB) signals, such as those generated by a real AE event.

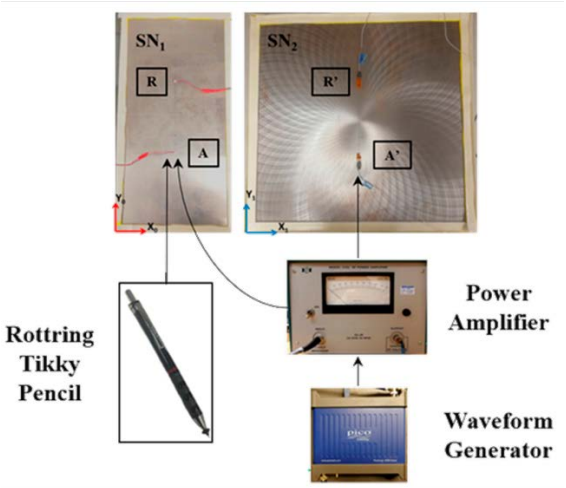

Figure 3.18 Experimental sensor networks: SN1 (Al) and SN2 (Steel).

The methodology used in the study has been divided into three phases for clarity:

- Analytical description of the proposed method (Phase I): the application of a FCTF to the TR method is described mathematically, thereby developing a strategy to reconstruct a generic BdB signal.
- Experimental Application (Phase II): The FCTF TR process is applied to experimentally measured data to reconstruct NBB and PLB signals from a thin aluminium sheet (1.6 mm thick), as well as to the reconstruction of NBB signals from a thick steel plate (13 mm thick). A sketch of the experimental set-ups is given in Figure 3.18, where sensor layouts are shown for the different materials. Two AE sources were used, namely, a Numerically Built Broadband (NBB) signal and a Pencil Lead Break (PLB).
- Computational Verification (Phase III): the analytical approach has been validated through a numerical model developed with SIMULIA ABAQUS that implements suitable model of the absorbing boundaries to minimize edge reflections. Some details of the modelling strategy are given in Figure 3.19. The TR process was applied to NBB and PLB signals.

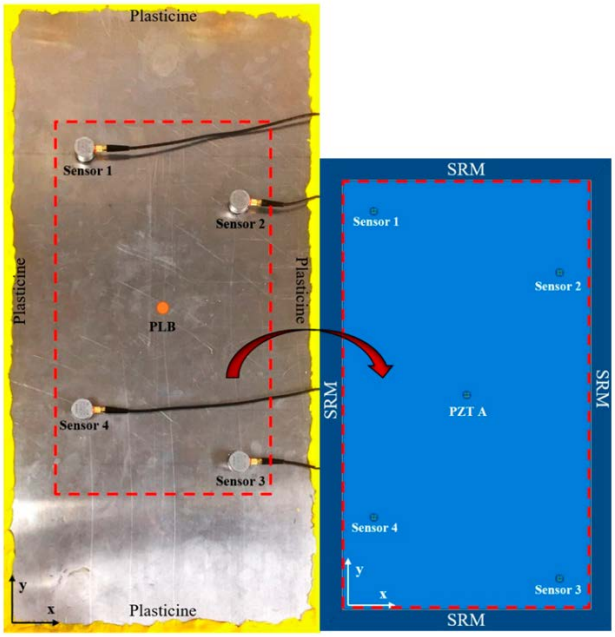

Figure 3.19 Comparison of the physical (on the left) and numerical (on the right) set-ups.

4 COMPOSITES AND FIBER METAL LAMINATES

4.1 Investigation on Disbond Arrest Features in adhesive joints (Univ. Bologna)

A Disbond Arrest Feature (DAF) is any design feature which can be used to retard or stop crack growth. For adhesively bonded joints this usually means stopping the crack growth in the adhesive layer, i.e. disbonding. DAFs are an attracting option to improve the fracture behaviour of adhesively bonded joints.

An investigation is in progress at the University of Bologna – Forlì Campus on fatigue crack growth in bonded GLARE specimens with a bolted disbond arrest feature; preliminary results have already been presented in the previous National Review.

The research is conducted on Cracked Lap Shear (CLS) modified by installing an Hi-Lok in the centre, as shown in Figure 4.1.

Figure 4.1 Bolted lap shear specimens (Flat and flush head Hi-Loks were used).

The CLS configuration allows to reproduce a mixed-mode ratio which is comparable to that found in real aeronautical components. All the tests have been conducted under fatigue tensile-tensile loading. The crack length was measured visually by a camera aimed at the specimen side and using an algorithm based on digital image correlation measurements. A 3D FE model of the bolted CLS specimen was also developed to compute the strain energy release rate (SERR).

The results of the fatigue tests show that the Hi-Lok has a retarding effect on disbond growth, as can be seen in Figure 4.2. The formation of secondary cracks in the GLARE adherends forced the tests to be stopped before a complete disbonding could occur. The numerical results are shown in Figure 4.3: the SERR distribution around the DAF changes significantly, with a reduction of mode I component and an increase of mode II component.

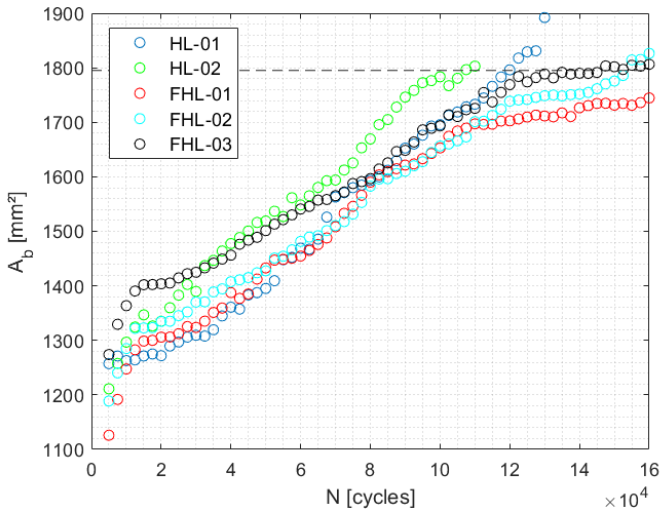

Figure 4.2 Fatigue crack growth measured by the digital image correlation algorithm. The horizontal dashed line marks the position of the Hi-Lok (HL = flat head FHL = flush head).

Furthermore, a model for prediction of disbond growth in adhesive joints with bolted disbond arrest features has been developed. The numerical 2-D model is based on a cohesive zone formulation, which has been implemented via a user-defined subroutine UMAT in the finite element software SIMULIA ABAQUS. Mixed mode disbonding was modelled through the Bürger's modification of Paris' law.

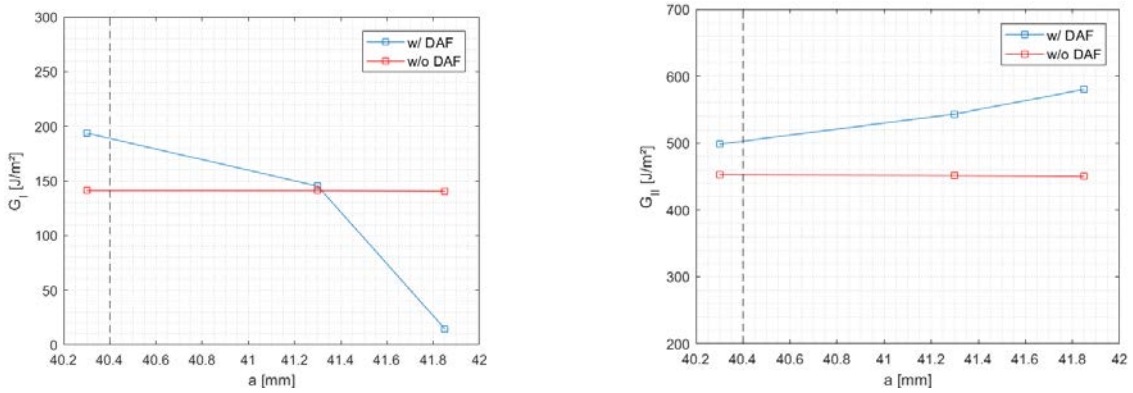

Figure 4.3 Strain Energy release rate evaluated by the finite element model. The two components of the SERR are shown: Mode I (left side), Mode II (right side).

Two test cases were simulated: a double cantilever beam (DCB) specimen and a modified cracked-lap shear (CLS) specimen with a bolted DAF. The results of the simulations for such cases were compared with experimental data and are shown in Figure 4.4 for the DCB specimen and in Figure 4.5 for the CLS one.

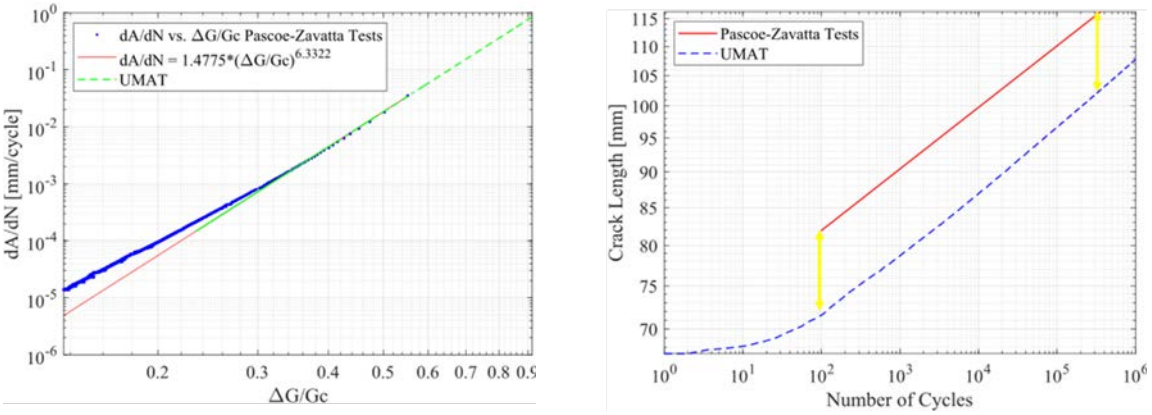

Figure 4.4 Comparison between simulation and experimental results for DCB specimen: Crack growth rate vs SERR ratio (left side), Crack length vs load cycles (right side).

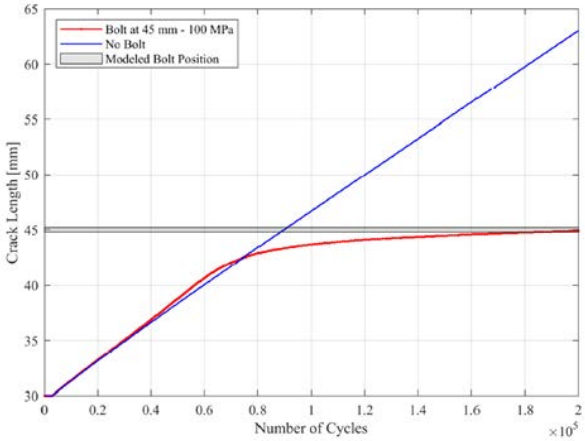

Figure 4.5 Crack length - number of fatigue cycles in CLS specimen with and without DAF under fatigue loading.

The results show that the models developed can reproduce well the observed fatigue disbonding and capture the disbond arrest provided by the DAF. Further studies on the behaviour of the crack front in presence of a disbond arrest feature shall be performed; since the 3D behaviour observed in experimental tests shows additional features, the development of a UMAT subroutine for the 3D case is envisaged.

4.2 Structural Health Monitoring by means of Optical Fibres (Uni. Bologna)

The use of optical fibre sensors (OFS) is diffused in the Structural Health Monitoring (SHM) community for their ability to detect many different physical quantities, its robustness against electromagnetic disturbances, its light weight and embedding possibilities. The last point has been widely investigated for different types of materials, but only recently the possibility to embed optical fibres in 3D printed structures has been considered. Additive Manufacturing (AM) offers new opportunities for the manufacturing of structures with complex geometries in a relatively short time. Moreover, new opportunities are offered by these manufacturing technologies, including innovative embedding solutions for different types of sensors.

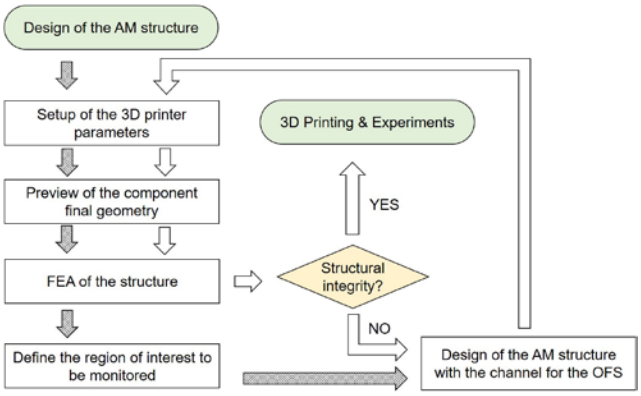

Figure 4.6 OFS embedding methodology in AM structures: logical flowchart.

Within the research program performed at the University of Bologna – Forlì Campus, embedding strategies for optical fibre sensors in structures produced with the Fused Deposition Modelling (FDM) were studied. Then a novel methodology to embed OFS was defined and tested through the production of specimens at three different filling densities and six different loads.

The original OFS embedding methodology and the experimental setup for its evaluation have been presented in the previous edition of the National Review; nevertheless, for sake of completeness and clarity, are shown in Figure 4.6 and in Figure 4.7, respectively.

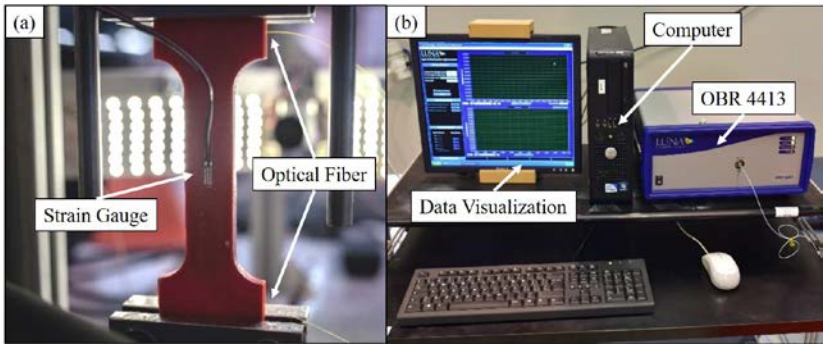

Figure 4.7 Test setup: specimen during the tensile test (a), and data acquisition system (b).

The experimental results, from specimens equipped with distributed OFS and strain gauges, were also compared with the data obtained from a numerical model developed in SIMULIA ABAQUS, in which the filling pattern of the specimens was accurately reproduced, highlighting both agreements and discrepancies with respect to the expected data. The comparison between measured and numerically assessed strains is shown in Figure 4.8.

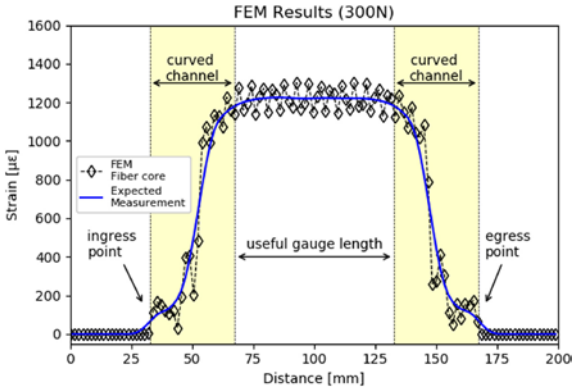

Figure 4.8 Numerical results at 300 N and 40% filling density.

4.3 Delamination onset resistance of composite material systems (Univ. Pisa)

Two aspects are important for the durability and damage tolerance of delaminated composites: the onset of fatigue delamination growth, described by strain energy release rate versus number of cycles (G-N curves), and the delamination growth rate, expressed in terms of a Paris diagram.

Although some damage growth is allowed by airworthiness regulations - provided the growth rate is slow, stable, and predictable - the helicopter community remains interested in using the no-growth approach due to the specific fatigue load spectra characterised by a very high number of cycles; in such cases the delamination growth onset approach is commonly used.

In this context, a collaboration between the University of Pisa and the Leonardo Helicopter Division has been set up with the aim of studying the phenomenon of the onset of delamination growth at a high number of cycles in a group of composite material systems commonly used in helicopter structures: the focus of the research has been on the assessment of the "endurance" limit that allows the designer to be confident of an infinite life, thus requiring long duration tests.

Material	Mode I (DCB)	Mode II (ENF)	Mode I+II (MMB)
UD AS4/8552	6	6	27
UD HTA/913C	13	19	28
5HS AGP280/8552S	17	18	5

Table 4.1 Number and type of fatigue tests performed.

Preliminary results from this research programme have already been documented in previous editions of the National Review and were presented more formally in a poster at ICAF 2019. In the meantime, some additional work has been carried out on the dataset, which is quite extensive as it includes 139 tests. These are Mode I, Mode II and Mode I+II fatigue tests for three different materials. In all cases, the tests were performed under displacement control, with constant displacement amplitude, characterised by a ratio of 0.1 between the minimum and maximum displacements. An overview of the number of specimens of each type tested is given in Table 4.1.

The additional data processing involved a refined fitting procedure to take into account the influence of run-outs on the values of the fitting curve parameters and on the standard deviation of each group of data. Scatter bands (of one standard deviation amplitude) were then added to the G-N curves. An example of the updated G-N curve plots is shown in Figure 4.9.

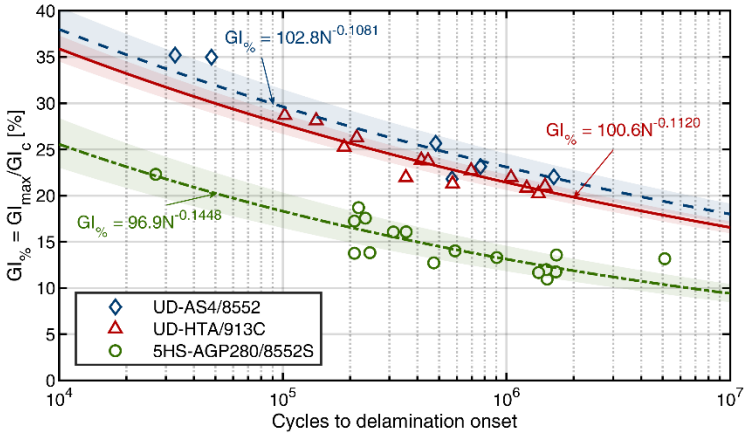

Figure 4.9 Mode I onset results normalized with G_{Ic} value for each material.

Finally, a fitting law, obtained by modifying the classical B-K law, was developped to satisfactorily interpolate the onset results at 10^7 cycles.

The modified B-K law for onset data is obtained by adding a linear correction term to the mode I contribution. The proposed relationship is described by the following equations, in terms of the mode mix ratio (G_{II}/G_{tot}):

$$G_{onset} = G^{I}_{onset} + G^{II}_{onset} \tag{4.3.1}$$

$$G^{I}_{onset} = G_{Io} - \alpha G_{Io}\left(\frac{G_{II}}{G_{tot}}\right) + G_{Io}\,(\alpha - 1)\left(\frac{G_{II}}{G_{tot}}\right)^{\gamma} \tag{4.3.2}$$

$$G^{II}_{onset} = G_{IIo}\left(\frac{G_{II}}{G_{tot}}\right)^{\gamma} \tag{4.3.3}$$

where G_{Io} and G_{IIo} are the pure mode I and pure mode II onset values respectively, while α and γ are fitting parameters. The results of the fitting of such model to the data of the two UD materials tested are shown in Figure 4.10.

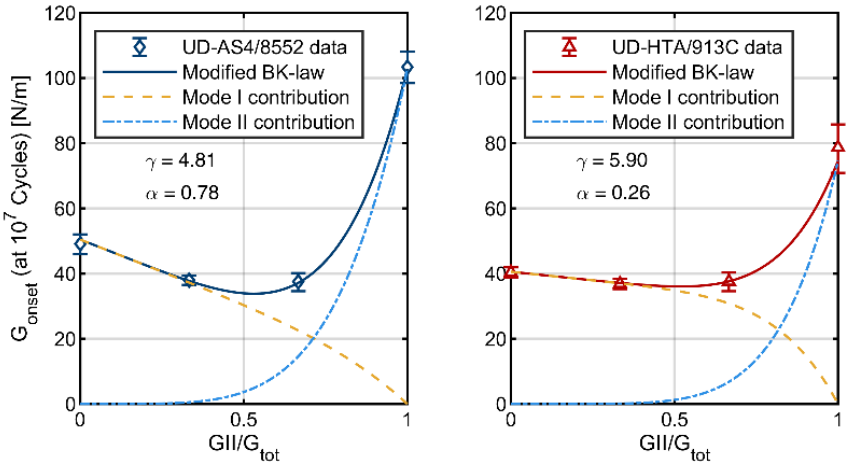

Figure 4.10 Fitting model for fatigue onset toughness vs. mode mix ratio.

The results for the fabric material are missing because they include only one mixed mode ratio and thus have only one valid point for the calibration the two fitting parameters, α and η.

By using the proposed fitting law, the fatigue onset performance of materials can be rationally compared. More details can be found in [1].

4.4 Meso-scale models for the interaction of damage modes in composites laminates (Milan Polytech.)

The response of complex composite aeronautical structures, such as rotorcraft rotors, is influenced by the evolution of different damage modes. A joint project between the Politecnico di Milano and Leonardo Helicopter has been undertaken with the aim of developing suitable numerical tools and analysis approaches to tackle the complex behaviour of damaged composite parts.

A ply-wise, bi-phasic FE modelling approach of the laminate is used, which allows the representation of both delamination and intralaminar matrix damage. The coupling between intralaminar cracking and delamination is introduced into the matrix constitutive law, without the need to refine the meshes at the sublayer level.

The proposed modelling approach is applied on simple specimens with cross-ply lay-up to assess its capability to capture both transverse matrix cracking and the interaction of intralaminar cracks with delaminations. The response of curved laminates with cross-ply lay-up then is studied to confirm the ability to capture transverse cracking and delaminations.

Representing the evolution of transverse matrix cracking in a finite element model requires three key elements: (i) residual thermal stresses induced by the curing process, (ii) stress increase

required for crack initiation due to the confinement effect of the adjacent layers, which resist crack opening (in-situ effect), and (iii) statistically distributed strength properties.

The first aspect was addressed by performing thermal stress analysis, simulating the cooling from cure temperature to ambient. The results showed that tensile transverse stresses can reach more than 60% of the transverse allowable.

For the in-situ effect, two models were evaluated. The first, valid for thin plies, links the in-situ transverse strength to the critical energy release rate transversal to the fibres and to the thickness of the group of transverse plies. The second model, more suitable for thick plies, evaluates in-situ transverse strength as proportional (by means of an amplification factor) to the transverse allowable for the homogeneous lay-up. An example of responses of the models for in-situ strength in shown in Figure 4.11.

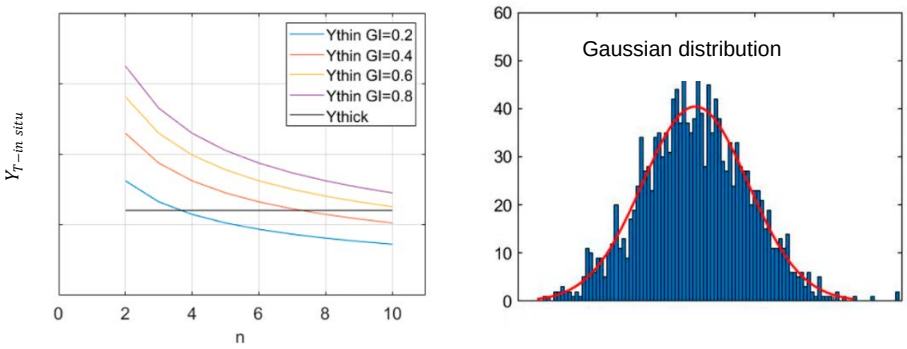

Figure 4.11 In situ strength of blocks made of n 90° oriented plies for different critical GI values (left side, GI in KJ/m^2) and an example of strength distribution (right side).

Gauss and Weibull distributions for strength were used. Parameters defining the shape of the distributions were selected through dedicated sensitivity studies and model tuning, while the in-situ strength was assumed as the distributions' mean value. An example of the gaussian distribution for strength is shown in Figure 4.11.

Notwithstanding the fine tuning of the model parameters, the tendency to saturation of crack density in the experiments cannot be completely captured. Improving the model in this respect requires the representation of the damage developed at the interfaces.

The proposed bi-phasic FE modelling approach offers the possibility of coupling interlaminar and intralaminar damage, thus allowing to mimic the presence of a transverse crack in the delamination evolution without a detailed representation of the stress state below the mesoscale level.

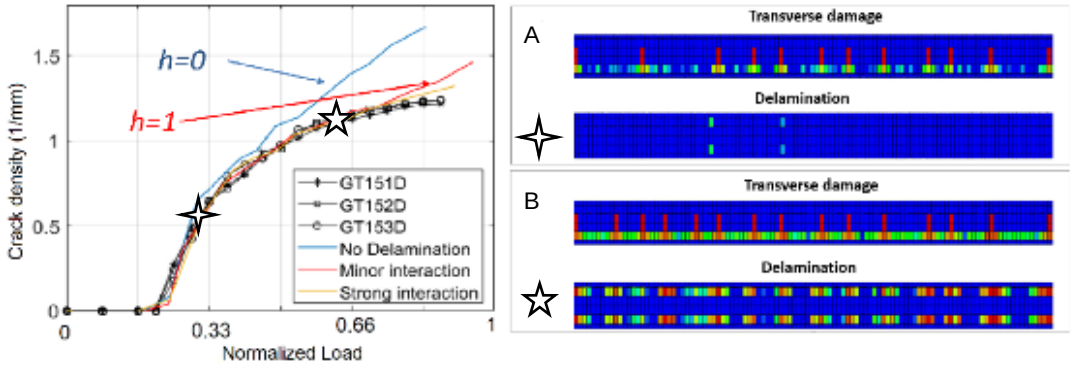

Figure 4.12 Numerical-experimental correlation of crack density with and without inter-intralaminar coupling (left side), contour of interlaminar and intralaminar damage at the onset of delamination (right side, A) and with diffused delamination damage (right side, B).

The coupling is obtained by reducing the mode II toughness and onset strength of the interface between plies as a function of the intralaminar damage developed in the matrix half-phases. A coefficient h modulates the coupling; h can be varied between 0 (no coupling) and 1 (maximum coupling).

The results presented in Figure 4.12 show that the application of a coupling coefficient allows a correct representation of the crack density evolution. All analyses include the effects of thermal residual stresses.

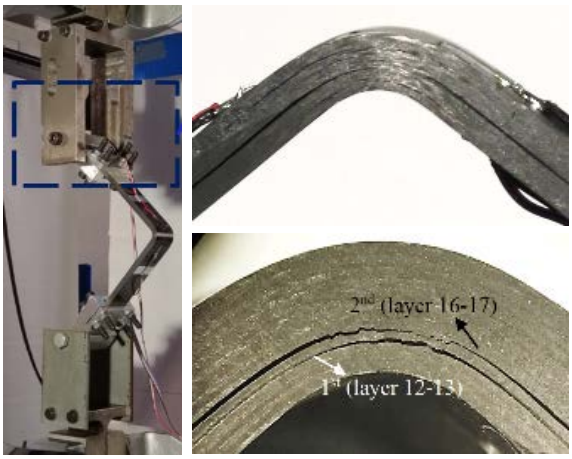

Figure 4.13 Experimental set-up for the angular specimens (left side), UD specimens failure mode example (right side, top), and cross-ply specimens failure mode example (right side, bottom).

Finally, the full numerical approach was used to model delamination and in-plane damage in angular composite specimens subjected to tensile loading. Two sets of specimens were fabricated from carbon/epoxy prepreg tape, a first set with UD lay-up and a second with cross-ply lay-up. The experimental set-up for the angular specimens is shown in Figure 4.13, together with examples of failure modes for both sets.

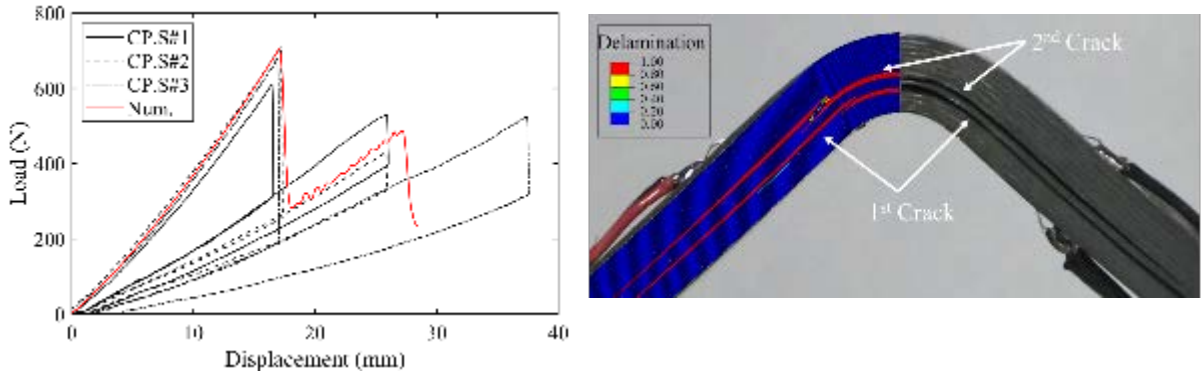

Figure 4.14 Numerical-experimental correlation for cross-ply specimen by adopting damage coupling: force vs. displacement curves (left side) and failure mode (right side)

An example of simulated results compared to the experimental one is shown in Figure 4.14. The comparison shows that the proposed approach can predict the loads required to nucleate and propagate damage in real structural elements with complex geometry and lay-ups.

The proposed mesoscale level models have been shown to be suitable for preliminary application in the design of critical details.

Further details can be found in the paper [2] to be presented at the 31st ICAF Symposium.

4.5 Testing of an out of autoclave–liquid resin infused carbon-epoxy curved stiffened panel (Univ. Pisa)

This research activity has been carried at the University of Pisa as a contribution to Task 12 of WP 1.1.2 of the Regional Platform of the European Union's Horizon 2020 Research and Innovation Programme Clean Sky 2. The University of Pisa participated to the programme as part of the AIRGREEN 2 cluster whose work was funded under Grant Agreement No 807089 – REG GAM 2018 – H2020-IBA-CS2- GAMS-2017; WAL (Work Area Leader): Leonardo Aircraft.

Task 12 was focused on the development of design approaches and manufacturing processes for primary structures of a regional aircraft in carbon/epoxy composites. The research is a joint effort of some of the members of the AIRGREEN 2 cluster, namely Hellenic Aerospace Industry (HAI) for the manufacturing activities, Leonardo Aircraft (LDO), the Italian Centre for Aerospace Research (CIRA) and the University of Naples "Federico II" (UNINA) for the introduction of impact damage and for the ultrasonic Non-Destructive Inspection (US NDI) and, finally, the University of Pisa (UNIPI) for the static and fatigue testing.

The reference structure chosen was a curved stiffened panel, representative of the outer wing box upper skin, produced by Liquid Resin Infusion (LRI) from dry preforms, then cured by an Out of Autoclave (OoA) process.

The following general requirements were defined for the Curved Panel (CP):

1) The panel shall be compliant with the "no growth" approach for BVID damage, under fatigue loading in compression at constant amplitude.
2) A Design Service Goal (DSG) of 60000 flights, a 1.5 Life factor, and a 1.15 Load Enhancement Factor (LEF) shall determine the number of cycles and the maximum cyclic load.
3) After the fatigue cycles the panel must retain a residual strength at least equal to the Design Ultimate Load (DUL).

Such general requirements, combined with the characteristics of the Test Article (TA) and the equipment available at the Aerospace Structures and Materials Laboratory of the University of Pisa (UNIPI), lead to the following specific requirements for mechanical testing:

- Potted ends with precision milled faces were required to ensure uniform compressive loading across the width of the panel.
- Due to the 3 stringers/4 spacing design adopted for the CP, lateral support devices were required to prevent premature buckling of the straight edges of the skin.
- Clamped boundary conditions at the rib feet (assumed in the design of the CP) were impossible to achieve in practice: alternative support options for the dummy ribs had to be devised.
- After selecting the fixture concept to support the dummy ribs and the skin sides of the TA, the effective UL of the test specimen had to be evaluated according to the buckling/failure load resulting from the test boundary conditions.
- Strain gauges had to be installed at suitably selected locations to monitor the delamination present in the TA according to the US scan performed by UNINA.
- Strain measurements were required after a block of fatigue cycles to detect changes in compliance due to possible delamination/damage growth.

Non-linear FE analyses of the test set-up were developed to support the fixture design and panel testing. The design of side and rib supports, inspired by the FE results, had the following features: the side supports had to be independent of the rib supports, the side supports had to be laterally stabilised and the rib edges had to be fixed to the frame of the testing machine.

As far as the side supports are concerned, their design is inspired to the constraint scheme adopted in the FE analysis and provides a local side support of the skin in each longitudinal bay of the edges. The design concept for the side supports is shown in Figure 4.15.

Each section of the edge is supported by steel bars which are held in place by a pair of AA alloy blocks fixed to the side bars (one on each side of the panel). Teflon strips are interposed between the steel bars and the panel to facilitate local longitudinal sliding of the edge under axial deformation caused by compressive loading. The side support blocks are held in place by composite steel section beams. Three-dimensional assembly drawings of the side supports are shown in Figure 4.15.

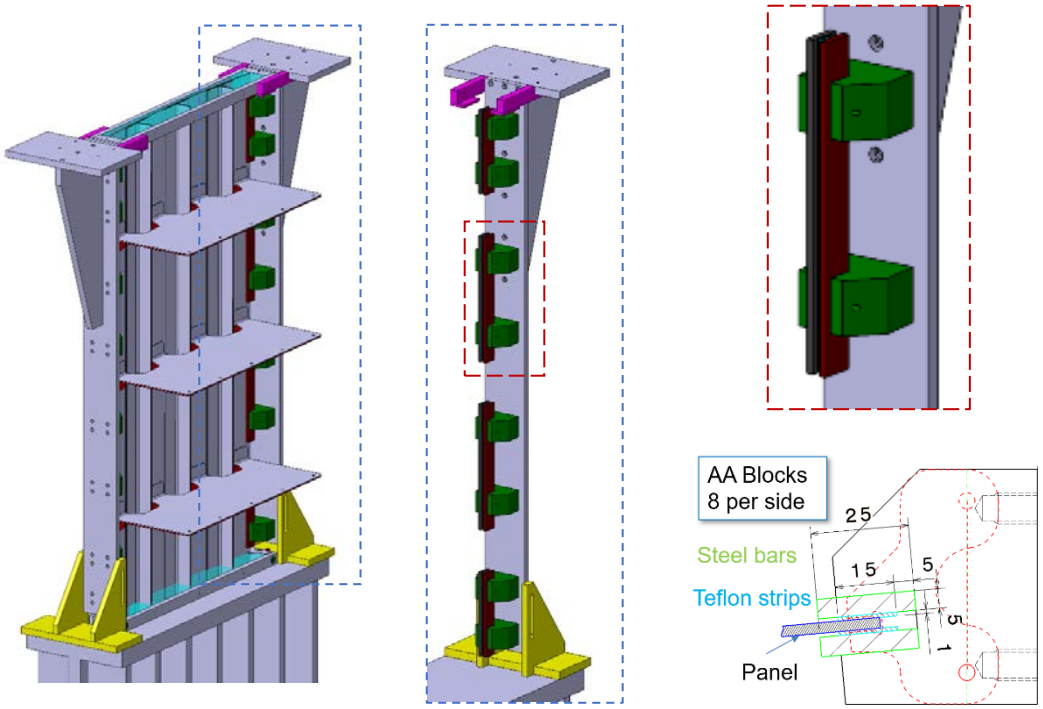

Figure 4.15 Concept and three-dimensional drawings for the side supports.

Given the characteristics of the panel and the nature of the mechanical test (compression fatigue plus static compression to failure), potted ends were required to protect the loaded edges from brooming and to ensure an adequate load introduction. Potted ends were installed, and precision milled to ensure planarity, mutual parallelism of the end faces and their orthogonality to the axes of the reinforcing stringers.

The panel was instrumented with 44 uniaxial SGs and 4 rosettes in a back-to-back configuration. SGs placed on the stringer attachment flange monitor strains in the vicinity of the stringer debonding caused by impact and measured during NDI. Four pairs are placed on the debonded zone and four on the outside of the boundary edges: this would capture potential delamination buckling and monitor possible damage growth during fatigue cycling.

The curved panel was mounted on a 3 MN servo-hydraulic fatigue testing machine and the specific support fixtures (side supports and rib end clamps) were installed. The panel mounted on the test machine is shown in Figure 4.16 with all the fixtures visible.

Due to the modified boundary conditions compared to the initial design, the buckling load of the panel, in its pristine condition, was re-evaluated by non-linear analyses (SIMULIA ABAQUS shell model with virtual SG). With a nominal buckling load of 500 kN the effective UL of the test article was set at 440 kN (13.6% margin) and, consequently, the effective LL was set at 293.3 kN.

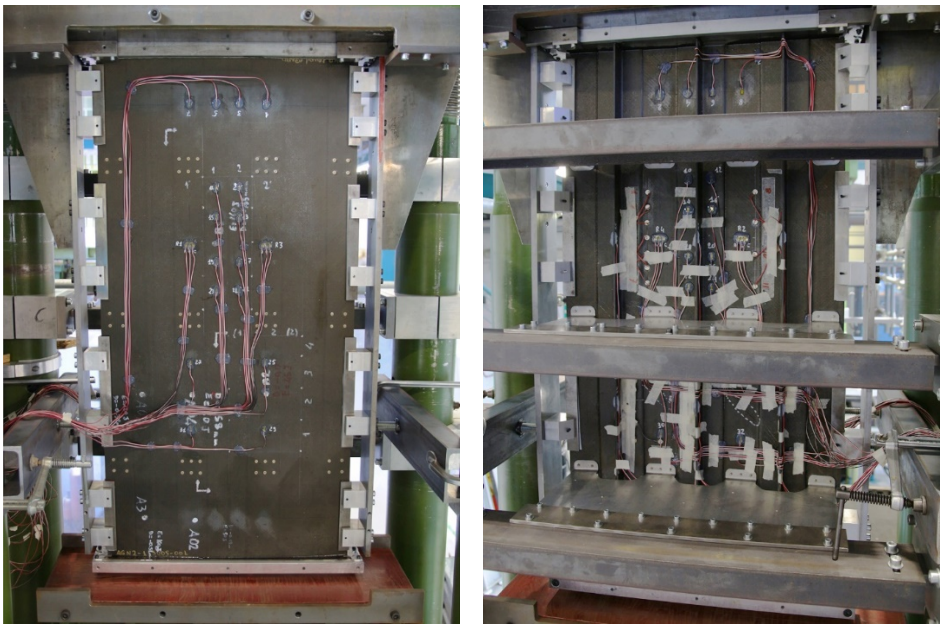

Figure 4.16 The curved panel mounted in the testing machine ready for testing.

Following the indication by Leonardo about the maximum cyclic load for a single equivalent cycle per flight (producing the same damage as all cycles in an average flight), the maximum fatigue load was assumed equal to LL (including a 1.15 LEF), with R=0.2. The number of flights was set at 90k (DSGx1.5).

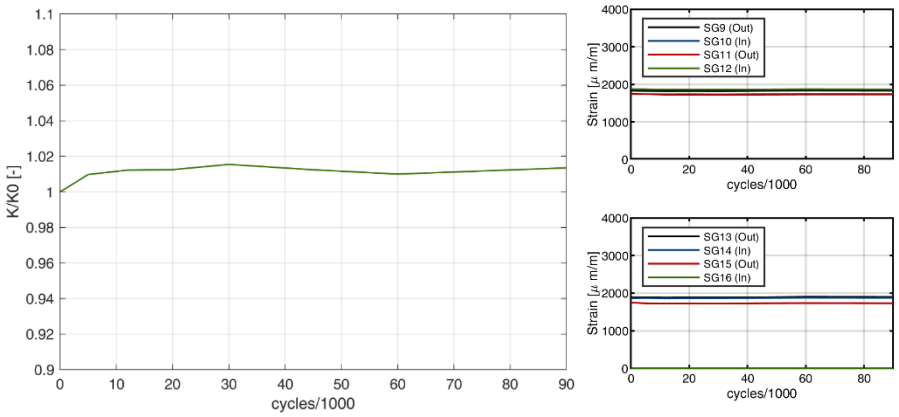

Figure 4.17 Variation with fatigue cycles of the axial stiffness K (on the left) and of the strain gauge reading close to the disbonding of the stringer (on the right)

The fatigue test was run at 0.5 cycles/sec and the test was stopped at 10k, 20k, 30k, 45k, 60k and 90k cycles to read the SGs and check for any variation in compliance.

Axial stiffness and selected strain values at LL for all the strain surveys are shown in Figure 4.17 as a function of completed fatigue cycles. The results confirm that any internal damage size did not change with fatigue cycling or, if it did, it did not cause any appreciable stiffness variation, either globally or locally.

Having demonstrated the ultimate load capability of the curved panel, a static load ramp (at the same loading rate of 100KN/min) was applied up to failure. The panel failed at an axial load of 457.6 KN that is approximately 4% above UL. Axial load vs. end-shortening behaviour and the failed panel are shown in Figure 4.18.

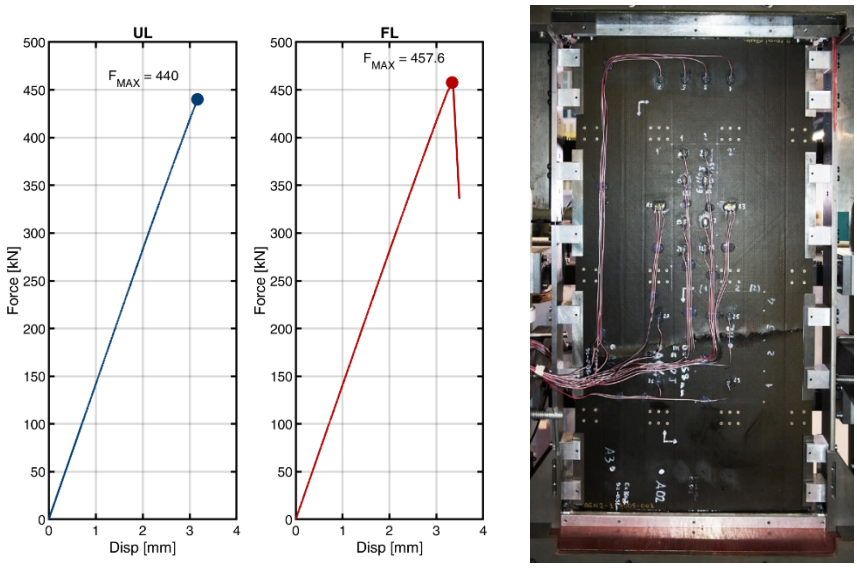

Figure 4.18 Axial load vs. end-shortening up to Ultimate Load (UL), and Final Failure (FF) after 90k fatigue cycles (left) and curved panel after final compression failure (1.04UL) (right)

Based on post-test images and strain gauge readings, it is likely that the failure was triggered by the interaction of skin buckling (evident in some of the inter-stringer bays) and the presence of impact damage in the lower bay.

5 NDI METHODS

5.1 Probability of Detection for Visual Inspection (Leonardo Helicopter Division)

A threat assessment**,** which includes the determination of the probable locations, types, and sizes of damage to be used in the fatigue tolerance evaluation, is required by 14 CFR§29.571 Amdt. 29-55 (2 December 2011) for each Principal Structural Element (PSE).

For Metallic Components of transmissions not exposed to damage in service, the minimum size defect that can be reliably detected by the relevant Detailed Visual Inspection (DVI) has been proposed as the maximum size defect that can remain undetected (Barely Detectable Flaw, BDF) in the PSE. Whenever the actual capability of a specific inspection method is questionable, the Probability of Detection (POD) as a function of damage size shall be assessed as per AC 29.571B (2 December 2011).

A Point Estimate Probability of Detection survey was therefore proposed by the Leonardo Helicopter Division for “half-penny” shaped artificial defects made in carburized steel mechanical components. Artificial defects were inflicted to the test specimens using Electro-Discharge Machining (EDM).

The Point Estimate is based on a defect length of 0.30 mm. The depth is determined as half of the length, to obtain the typical semi-circular cross section used in the damage tolerance analysis. The width is determined as the smallest that can be achieved with EDM, and it is consistent with the width of real case scratches on metallic components. Examples of such scratches are shown in Figure 5.1.

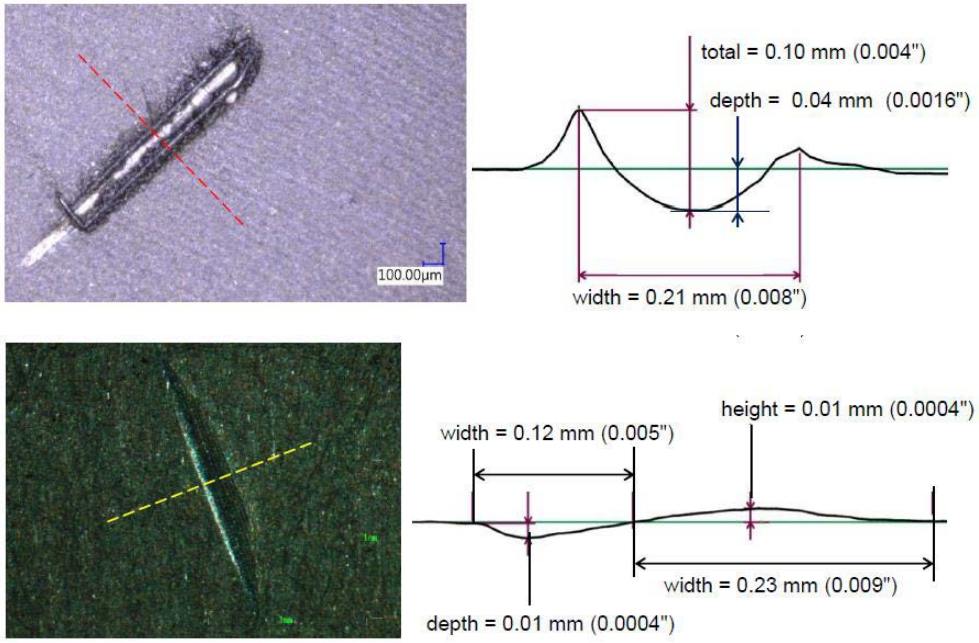

Figure 5.1 Examples of real case scratches on metallic components.

A reliably detectable flaw has been defined as the flaw that can be detected with a 90% probability of detection at a 95% confidence level ($POD_{90\text{-}95}$).

The binomial distribution of probability (appropriate for the Hit/Miss visual inspection data) is used to determine the number of successes (Hits), out of the total number of trials, that provides a 90% probability of success with a 95% lower confidence bound. Results are shown in Table 5.1.

Number of trials	Number of hits	Number of misses
29	**29**	**0**
46	45	1
61	59	2

Table 5.1 Hits per number of trials that yield a 90% probability of success at 95% confidence.

A total of 29 artificial defects have been inflicted on 10 different gears (actual aircraft components). Test specimens have been selected based on the worst-case surface finishing for defect visibility. The defects are randomly distributed on the test specimens, from a minimum of 0 defects to a maximum of 4. Such defects were added to all the defects naturally present on the selected components and the actual size for each defect has been evaluated by making silicon rubber patterns. Some examples of the artificial defects used for the PoD assessment are shown in Figure 5.2.

The test specimens were inspected by 3 different inspectors qualified to carry out the DVI for Transmission Metallic Components, using the same tools and procedures used during manufacture. The inspectors were blind to the purpose of the inspection, the number and location of the artificial defects, and the natural defects present in the specimen were not considered. The survey gives a positive result if all 29 artificial defects are found. Each finding is considered independent, and all inspectors were required to find all 29 defects to ensure that inspector variability is accounted for.

Each inspector used only the tools contained in the standard visual inspection toolbox to inspect the samples and all findings (artificial and natural defects) were recorded on the inspection report cards.

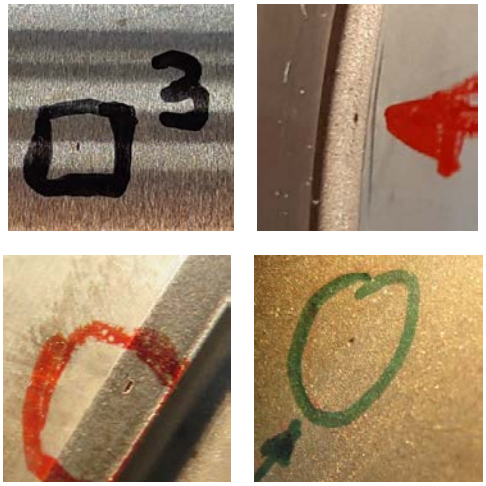

Figure 5.2 Examples of artificial defects used for the PoD assessment.

The number of the natural defects identified was different because some of them were produced during the survey by handling (dents/nicks/scratches) or by exposure to external agents (corrosion); others, with negligible depth, which could be easily eliminated by means of manual polishing, were highlighted or not on a basis of personal judgement.

All the 3 inspectors were able to detect 29/29 artificial defects inflicted without any misses as shown in Table 5.2. Based on this survey, it was possible to claim a $POD_{90\text{-}95}$ for DVI inspections in case of 0.30 mm long - 0.15 mm deep defects.

item	No. of artificial defects	Defect #	Inspector #1		Inspector #2		Inspector #3	
			No. of findings	hit/miss	No. of findings	hit/miss	No. of findings	hit/miss
#A	4	1	26	HIT	35	HIT	32	HIT
		2		HIT		HIT		HIT
		3		HIT		HIT		HIT
		4		HIT		HIT		HIT
#B	3	5	8	HIT	15	HIT	19	HIT
		6		HIT		HIT		HIT
		7		HIT		HIT		HIT
#C	4	8	14	HIT	16	HIT	23	HIT
		9		HIT		HIT		HIT
		10		HIT		HIT		HIT
		11		HIT		HIT		HIT
#D	2	12	5	HIT	6	HIT	10	HIT
		13		HIT		HIT		HIT
#E	3	14	6	HIT	10	HIT	12	HIT
		15		HIT		HIT		HIT
		16		HIT		HIT		HIT
#F	4	17	5	HIT	17	HIT	18	HIT
		18		HIT		HIT		HIT
		19		HIT		HIT		HIT
		20		HIT		HIT		HIT
#G	3	21	5	HIT	6	HIT	10	HIT
		22		HIT		HIT		HIT
		23		HIT		HIT		HIT
#H	0	-	2	HIT	2	HIT	8	HIT
#J	4	24	8	HIT	15	HIT	19	HIT
		25		HIT		HIT		HIT
		26		HIT		HIT		HIT
		27		HIT		HIT		HIT
#K	2	28	4	HIT	5	HIT	11	HIT
		29		HIT		HIT		HIT
TOTAL		**29**	**83**	**29**	**128**	**29**	**162**	**29**

Table 5.2 POD Survey Results.

6 AIRCRAFT FATIGUE SUBSTANTIATION

6.1 Fatigue related activities on AW189 (Leonardo Helicopter Division)

In the following, some examples of the fatigue life reassessment for AW189 components are given, they are a completion of similar activities already reported in previous version of the National Review. Improved fatigue evaluations were carried out for extended performances and the new limitations were reported in the Helicopter Maintenance Manual as appropriate.

For the AW189 helicopter equipped with Safran Engines (AW189K) an extension of the Service ceiling altitude up to 15000ft was obtained (at 8,600 kg MTOW). Other improvements of the same configuration include:

- Take off and landing envelope extended to 14,000 ft
- Rescue pickup & release operations extended up to 10,000 ft
- Cargo hook pick-up & release operations extended up to 10,000 ft
- flight envelope with cargo loaded extended up to 12,000 ft

Reduction of maintenance costs was obtained also because of the life extension of the Tail Rotor Hub and of Main Landing Gear & Nose Landing Gear attachments on main cabin. For the first a Flaw Tolerance Safe Life approach was used, in the second case full scale test was performed (the fatigue test is ongoing even though the life extension has been already achieved).

As far as components improvement is concerned, a new Upper Rod End of the Pitch Link for the Main Rotor has been developed. Changes in the manufacturing process of the elastomer have been validated maintaining the original elastomeric material.

A new Tail Gearbox Fitting was also designed for life increase that is currently in the certification process.

6.2 EUROFIGHTER Production Major Airframe Fatigue Test (Leonardo Aircraft Division)

The PMAFT was a full-scale test which aimed to provide evidence of airframe durability by demonstrating a fatigue life of 18000 hours for the Eurofighter Aircraft. Since a design scatter factor of 3 is used, at the end of the test, a clearance for a 6000 Flight Hours fatigue life will be issued for the EFA.

The test items were loaded by actuators, which reproduced the manoeuvres defined by the Composite Set of Training Missions (CSTMs). The fatigue test, performed in Brough (UK), was completed in 2018.

SFH	Part	Damage Description	Representative
15000	Rear Fuselage Upper Panels XXXXX	Delamination occurred in different ten new locations	yes
15000	RH Tip Pod - OB Front Spar Attachment Lug	Attachment lug bush XXXXXXXXXXXX had migrated forward	yes
17209	RH Wing Rib XXXXX Machined Part	ITSPL right I/B Pylon Housing that have been found cracked	TBD (pending results of Tear Down Analysis)
18000	LH Wing Rib XXXXX Machined Part	ITSPL left I/B Pylon Housing that have been found cracked	TBD (pending results of Tear Down Analysis)
18000	Rear Fuselage Panel XXXXX	One of the attachment bolt grommets had become detached from the panel XXXXX (LHS)	no
18000	LH Wing Fixed Leading Edge Landing	Cracks were found in the LHS fixed leading edge assembly on the lower wing skin closing plate panel landing XXXXXXXXX	no
18000	RH Wing Fixed Leading Edge Landing	Cracks were found in the RHS fixed leading edge assembly on the lower wing skin closing plate panel landing XXXXXXXXX	no
18000	RH Wing Removable Panel XXXXXXXXX	Panel (XXXXXXXXX) was mechanically damaged by the inboard R/H side slat track lug	no
18000	LH RH Wing Rib XXXXX Machined Part (OB stud housing)	LH Outboard stud housing was found to have crack like indications at 3 locations	TBD (pending results of Tear Down Analysis)

Table 6.1 EFA fatigue test damages on the wings occurred between 15000 and 18000 Test Hours.

Since the Leonardo Aircraft Division has the System Design Responsibility (SDR) of the wings, the Fatigue Office in Turin was tasked to justify all the damages occurred on the left wing. In the period covered by this National Review, Leonardo Fatigue Office has been working on the explanation of the wing fatigue damages occurred between 15000 and 18000 Test Hours. All the relevant damages are shown in Table 6.1.

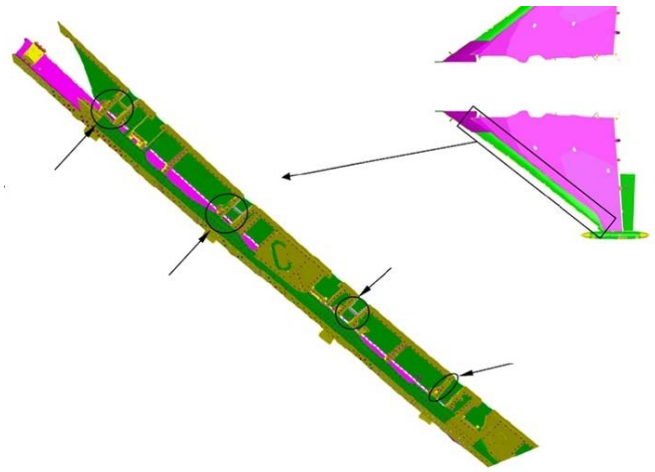

Figure 6.1 FEM model for the analysis of cracks on the Fixed Leading-Edge Landing

Major inspection fatigue cracks were found in the LHS fixed leading edge Landing. To investigate the damages the following approach was used:

- Study of the geometry of the landing and the actuators involved.
- Study of the loading from files that contain the registrations of actuators forces (.dac files).
- Study of the most demanding static cases by means of FEM (see Figure 6.1)
- Study of the crack propagation (NASGRO) under load time history provided by .dac files.

The Fatigue Analysis did not highlight specific issues for this part and the fatigue cracks were attributed to an error during the production of the wing (lack of shim between two parts, which increased the stresses in the area nearby).

6.3 M346 & M345 Trainers Certification status (Leonardo Aircraft Division)

M346 and M345 are Trainer aircrafts developed by Leonardo Aircraft Division, the first is an advanced trainer for combat pilots while the second is a jet aircraft designed for low cost, basic, through to advanced, training (see Figure 6.2).

The M-346 is a twin-engine, tandem-seat aircraft with fully digital flight controls and avionics. It is equipped with a fly-by-wire flight control system with quadruple redundancy, a modern human-machine interface with Head-Up and Multi-Function Displays, Hands On Throttle And Stick controls.

The M-345 is a jet aircraft equipped with modern avionics and characterised by operating costs comparable to those of a high-powered turboprop trainer. Based on experience in the M-346 programme, the avionics of the M-345 include a state-of-the-art man-machine interface, while the Embedded Tactical Training System (ETTS) permits reproduction of highly complex tactical scenarios during training flights.

Both aircrafts have completed the fatigue analysis process (Durability & Damage Tolerance) and the relevant fatigue models for fleet monitoring and the inspection plan have been developed according to their Design Spectrum.


Figure 6.2 Leonardo Aircraft Division Trainers: M346 (on the left) and M345 (on the right)

The aircrafts share the same certification basis, that is a Durability approach, with a scatter factor of 2, applied to the life demonstrated by means of a Full-Scale Fatigue Test. Fatigue Tests on major components are ongoing according to data in Table 6.2.

M 345 trainer A/C	
Item	**Completion**
Wing	20 %
Fuselage + Vertical tail	5 %
Hor. Tail + Equilibrator	56 %
Rudder	10 %
Ailerons	5 %
Flight Control	initial phase

M 346 trainer A/C	
Item	**Completion**
Wing	25 %
Fuselage	50 %
Stabilator	85 %
Vertical Tail + Rudder	60 %
Ailerons	100 %
Flap	100 %

Table 6.2 Trainer aircrafts Fatigue Tests status.

6.4 FALCO XPLORER – Full Scale Fatigue Test (Leonardo Aircraft Division)

The Falco Explorer is a new UAV bring designed by the Aircraft Division of Leonardo company. It is characterized by a high aspect ratio wing and a V tail as shown in Figure 6.3.

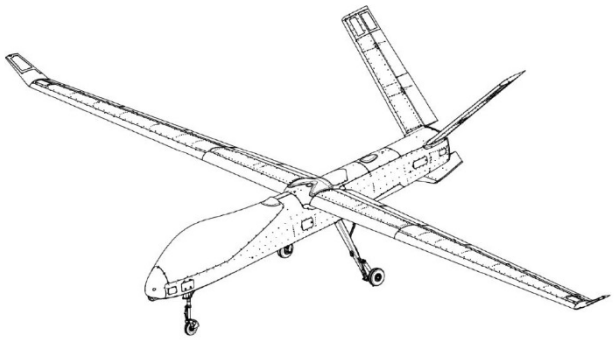


Figure 6.3 Leonardo Aircraft Division Falco Explorer UAV

The airframe will undergo a full-scale fatigue test to assess the performances of the metallic and composite components. The design activity is divided into Work Packages (WP) and the fatigue test is comprised in WP3 which is under the responsibility of the Turing Fatigue Office.

Currently, the attention is focused on the initial study phase of the full-scale fatigue test for the wing alone.

To this end, all the possible design mission profiles of the aircraft are incorporated into an equivalent test mission profile, which has only three main phases for the in-flight loads (climb, cruise, and descent) and the taxi and sink speed spectra for ground loads.

The idea under the development of the test mission profile is sketched in Figure 6.4.

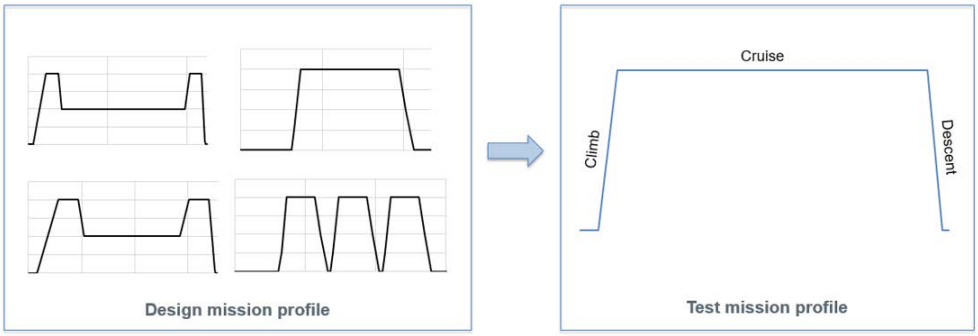

Figure 6.4 Falco Explorer UAV test mission profile for full-scale fatigue tests

7 REFERENCES

[1] Boni L., Fanteria D., Lazzeri L., Mariani U., Rigamonti M. (2022): Delamination onset in composite materials due to fatigue loading, Journal of Composite Materials, 56 (16), 2585–2598.

[2] Ghiasvand S., Airoldi A., Sala G., Aceti P., Ballarin P., Baldi A., Mesiani E. (2023): Meso-scale models to analyse the interactions of damage modes in composites laminates, 31st Symposium of the International Committee on Aeronautical Fatigue and Structural Integrity, Delft (The Netherlands), 26-29 June 2023.